2-9-2010

Investigation of CO2 insertion into lanthanide amides, alkoxides, and mixed amide/alkoxides

Leigh Anna M. Ottley

Follow this and additional works at: https://digitalrepository.unm.edu/chem_etds
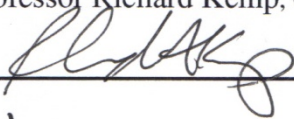
Leigh Anna M. Ottley
Candidate

Chemistry and Chemical Biology
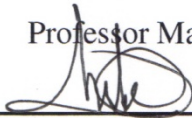*Department*

This thesis is approved, and it is acceptable in quality
and form for publication:

Approved by the Thesis Committee:
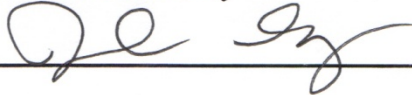
Professor Richard Kemp, Chairperson
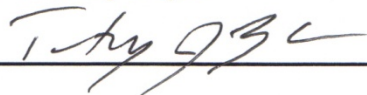
Professor Martin Kirk

Professor John Grey

Dr. Timothy Boyle

INVESTIGATION OF CO$_2$ INSERTION INTO LANTHANIDE
AMIDES, ALKOXIDES, AND MIXED AMIDE/ALKOXIDES

BY

LEIGH ANNA M. OTTLEY

BACHELORS OF SCIENCE IN CHEMISTRY
University of New Mexico

2006

THESIS

Submitted in Partial Fulfillment of the
Requirements for the Degree of

**Master of Science
Chemistry and Chemical Biology**

The University of New Mexico
Albuquerque, New Mexico

December, 2009

To my loving family and friends for their encouragement and support throughout all my endeavors.

ACKNOWLEDGEMENTS

INVESTIGATION OF CO_2 INSERTION INTO LANTHANIDE
AMIDES, ALKOXIDES, AND MIXED AMIDE/ALKOXIDES

BY

LEIGH ANNA M. OTTLEY

ABSTRACT OF THESIS

Submitted in Partial Fulfillment of the
Requirements for the Degree of

**Masters of Science
Chemistry and Chemical Biology**

The University of New Mexico
Albuquerque, New Mexico

December, 2009

INVESTIGATION OF CO_2 INSERTION INTO LANTHANIDE AMIDES, ALKOXIDES, AND MIXED AMIDE/ALKOXIDES

Leigh Anna M. Ottley

B.S., Chemistry, University of New Mexico, 2006

M.S., Chemistry and Chemical Biology, University of New Mexico, 2009

ABSTRACT

A novel set of lanthanide (Ln) alkoxycarbonates, $[Ln(\mu\text{-}CO_2\text{-}DBP)(DBP)_2]_2$

where Ln = lanthanide; and DBP = $OC_6H_3\text{-}2,6\text{-}C(CH_3)_3$, were isolated from a systematic

study of the insertion of $CO_{2(g)}$ (referred to as CO_2) into the Ln-O bonds of a series of

new lanthanide alkoxides, $Ln(OR)_3$. This study was undertaken to determine if the

deleterious metal carbonate $[M(CO_3)_y]$ formation that promotes higher thermal budgets

during processing could be avoided. While processing controls can reduce the formation

of the $M(CO_3)_y$ phases, this is not always effective, and preventing the formation of these

phases is of interest. Since CO_2 insertion into transition metal alkoxides has been

extensively studied and many structures reported, this research focused on CO_2 insertion

into the less-studied Ln-O bonds of $Ln(OR)_3$. Initially a series of lanthanide amides

$[Ln(NR_2)_3$ where R = $SiMe_3$ and Ln = Ce **(1)**, Sm **(2)**, Dy **(3)**, Yb **(4)**, and Lu **(5)**$]$ were

synthesized following established routes.[4-6] Subsequent conversion of the $Ln(NR_2)_3$

species into a series of $Ln(OR)_3$ was achieved by an amide/alcohol exchange route

resulting in $Ln(DBP)_3$ (Ln = Ce **(6)**, Sm **(7)**, Dy **(8)**, Yb **(9)**, and Lu **(10)**; DBP = 2,6-di-

tert-butylphenoxide).[7, 8] Once isolated, CO_2 at low pressure (<5 psig) and ambient

temperature was introduced to the $Ln(OR)_3$ species to form a novel family of lanthanide

alkoxycarbonate compounds identified as $[Ln(\mu\text{-}O_2C\text{-}DBP)(DBP)_2]_2$ (Ln = Ce **(11)**, Sm

(12), Dy (13), Yb (14), and Lu (15)). Surprisingly, CO_2 did not insert into all of the Ln-O bonds, indicating that this process might be more controllable than initially expected. Higher-pressure CO_2 experiments yielded the same carbonate compounds. Further manipulation of the ligand set, as a means to control CO_2 insertion, was explored by using a mixed amide/alkoxide precursor generated *in situ*. This resulted in the formation of an unusual complex, $Sm_4(\mu\text{-}CO_3)_2(\mu\text{-}O)_2(DBP)_4(THF)_2(\mu\text{-}DBP)$ **(16)**. From this fundamental study, it has been shown that the ligand may be able to impact the degree of CO_2 insertion into Ln-O bonds. The synthesis and characterization of **1 - 16**, as well as future implications of this work, will be discussed in detail.

Table of Contents

LIST OF FIGURES

LIST OF TABLES

1. Introduction

1.1   M(OR)$_x$ Precursors Conversion to M(CO$_3$)$_y$

It is widely reported that metal alkoxides [M(OR)$_x$] are excellent precursors to ceramic materials due to their high solubilities, low thermal decomposition temperatures, high volatilities, commercial availability, and ease of crystallization. However, upon calcination of these M(OR)$_x$ precursors into the desired metal oxides, metal carbonates [M(CO$_3$)$_y$] are often formed. This is a result of gaseous carbon dioxide [termed CO$_2$] insertion into M-OR bonds. The problematic CO$_2$ is available in large quantities from the ambient atmosphere (average concentration of about of 383 parts per million by volume),[9] but can often be reduced by processing under inert atmospheres. However, this increases the cost of production and is not completely effective, due to the CO$_2$ produced by the decomposition of the hydrocarbon ligand moiety. The higher processing temperatures required to convert M(CO$_3$)$_y$ to the desired ceramic material affects numerous materials.

One example of a system that suffers from this problem is in the production of the superconductor yttrium barium copper oxide thin films (YBCO). Upon calcination, conversion of the M(CO$_3$)$_y$ intermediate phases that form require temperatures well above 800 °C to crystallize the desired YBa$_2$Cu$_3$O$_{7-x}$ (PDF No. 39-1496) phase of YBCO. [10-12] These higher processing temperatures result in unwanted reactions between the substrate supports and the YBCO thin film. Typically, the deposition of a buffer layer is used to circumvent this problem, thus raising the cost of the final product. Another example where M(CO$_3$)$_y$ formation is a problem is the production of perovskite (ABO$_3$) phase of

barium titanate ($BaTiO_3$). The precursors used to synthesize $BaTiO_3$ initially decompose into two phases, $BaCO_3$ and TiO_2. As the temperature increases, these materials calcine into the oxycarbonate, $Ba_2Ti_2O_5CO_3$. Once formed, temperatures of the magnitude 700-800 °C must be used to obtain the desired $BaTiO_3$.[11] The higher temperatures can be attributed to the slow decomposition kinetics of the oxycarbonate phase.[11] One method to prevent $M(CO_3)_y$ formation in these materials is to use fluorinated species, such as trifluoroacetate, which forms an oxy-fluoride intermediate, avoiding the $M(CO_3)_y$.[10] While the oxy-fluoride material can be converted at lower temperatures it comes at the cost of generating several undesired gases [*i.e.*, HF, $F_2(g)$] or contaminating the final ceramic with fluorine.

Due to the need to eliminate carbonate formation for ceramic materials applications (*vide infra*), the ability to control or prevent CO_2 insertion into M-L (where L = ligand) bonds is of great interest. Transition metal complexes have been well studied for CO_2 insertion into M-L bonds for this and other interests.[13-15] Recently, lanthanide (Ln) compounds for the production of ceramic materials have become of interest due to the unique properties that these cations can impart on the final material. This research project focused on investigating the CO_2 insertion into Ln complexes to develop a fundamental understanding of the reactivity of this special class of compounds.

1.2 Interest of CO₂ Insertion into Lanthanide Complexes

The interest in Ln cation in ceramic materials derives mainly from the so-called 'lanthanide contraction,' which describes systematic changes in the atomic radii that maintain a +3 oxidation state as the series is traversed.[16, 17] These cations also exhibit a

systematic change in electronegativity because the Ln's have valence electrons located in the 4f-orbitals that allow further fine-tuning of the electronic properties. However, the f-orbitals are 'buried' in comparison to the d-orbitals and this fact, coupled with their small overlap with ligand atom orbitals, attaches a predominantly ionic character to Ln-ligand atom bonds in compounds.[18] Thus, the mainly electrostatic interactions between the Ln cations and the hetero-atoms of the ligands result in irregular geometric arrangements, and a wide range of coordination numbers have been reported (3-12). The shapes of the f-orbitals tend to be spherical and less directional than p- and d-orbitals. This could cause substantially different reactivity than noted for the transition metals.

Several materials applications have taken advantage of this unique family of cations for use as precursors or dopants. For instance, a series of $Ln(OR)_3$ were successfully employed as dopants in lead zirconium titanate (PZT) to decrease the fatigue behavior in this material.[7] In addition, Ln dopants have been found to increase luminosity for bio-imaging agents (*i.e.*, upconvert materials) that mimic naturally occurring fluorescent minerals (NOFs). [19, 20]

As the use of Ln compounds, in particular $Ln(OR)_3$, increases for the production of tailored ceramic materials, carbonate formation again becomes an issue. Few studies concerning the reactivity of CO_2 and $Ln(OR)_3$ are available.[21] Therefore, it is not surprising that there are no crystallographically characterized $Ln(O_2COR)_3$ compounds reported that resulted from insertion of CO_2 into Ln-OR bonds. However, several dinuclear La-Zn, Gd-Cu, and Tb-Cu complexes have been characterized that possess methylcarbonato ligands, (O_2COMe). The carbonato ligand evolved from the reaction of CO_2 and methanol or alternatively was a product of reaction with monomethylcarbonate

ligands. Again, none of these compounds were synthesized by CO_2 insertion into a M-O bond.[22, 23]

Therefore, the focus of this research was to exploit the unique qualities of Ln cations to undertake a systematic investigation of CO_2 insertion into $Ln(OR)_3$ compounds. This study explored the fundamental reactivity of these precursors to small molecule insertion reactions and attempted to determine whether this is a controllable process. Since there are 14 Ln cations in the series, it is unreasonable to undergo a study involving all of these compounds; therefore, a more manageable subset of 5 cations spanning the series was selected (Ce (1.818 Å), Sm (1.80 Å), Dy (1.78 Å), Yb (1.76 Å), and Lu (1.74 Å).[16] The variables explored for insertion of CO_2 into Ln-element bonds included the cation size, the identity of the ligand, and the steric bulk of the ligand. With this basic understanding, provided in this study, it is anticipated that prevention of lanthanide carbonate formation, very useful for the processing of these precursors, can be achieved. As well, this may lead to increase in the number of ceramic material systems that employ Ln cations.

1.3 *Mechanisms of CO$_2$ Insertion into Bonds*

CO_2 is a unique small molecule that has an electrophilic carbon center with nucleophilic oxygen atoms, allowing it to undergo a wide range of reactions. This reactivity can be detrimental for materials production, as CO_2 readily inserts into $M(OR)_x$ bonds during thermal processing (*vide infra*). Therefore, understanding how, where, and when CO_2 inserts into specific bonds will provide fundamental reactivity information that can be exploited to control this reactivity. CO_2 has been found to insert into seven types of metal-element (M-E) bonds where E = H, C, N, O, P, Si or another metal, to form what

is considered the normal insertion product (top) or the abnormal insertion product (bottom) **(Figure 1)**.[3] The element attached to the M in the starting material dictates what the insertion product becomes (*i.e.*, if E = H, then the insertion product can be the formate or metallocarboxylic acid complex; E = C, carboxylate or a alkoxycarbonyl complex; E = N; carbamate; E = O, carbonate).[3]

Figure 1. CO_2 insertion into M - E bonds. [3]
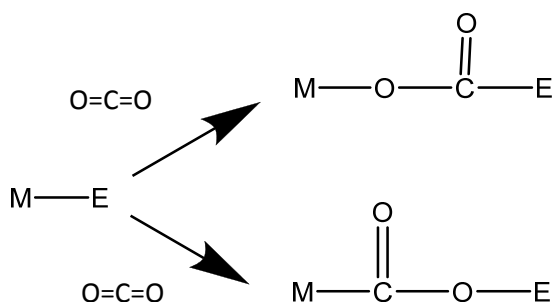
There are many examples of insertion into M-H, M-C, M-N, and M-O bonds (where M = transition metal), but a lacuna exists for Ln-N and even more specifically Ln-O bonds.

The products that are obtained from insertion of CO_2 into a M-OR where R= alkyl or aryl are termed carbonato ligands (O_2COR), while for R = H it would be termed hydrogen carbonato.[1-3] Three binding modes have been observed for carbonato ligands in mono or dinuclear transition metal complexes a) η^1, b) η^2, c) μ_2-η^2 (**Figure 2**). These are in comparison with the well studied bonding modes of carbamate (O_2CNR_2) ligands minus a μ_2-η^3 mode.[1-3]

Figure 2. a) η^1, **b)** η^2, **c)** μ_2-η^2. Carbonato ligand binding modes to either a mononuclear or dinuclear metal atom .[1-3]

a)   b)   c)
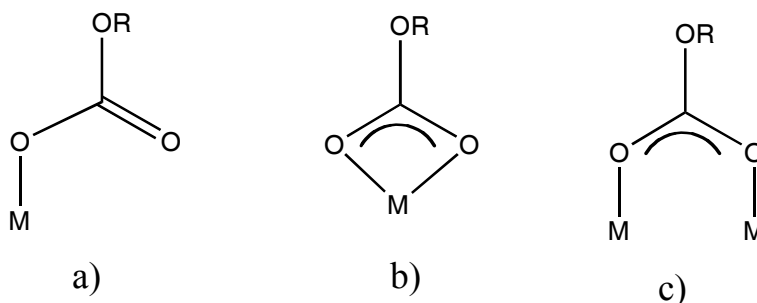
1.4 Families of Lanthanide Compounds Selected for this Study

Three sets of lanthanide complexes were synthesized and characterized for this research: amides $\{[Ln(SiMe_3)_2]_3\}$, alkoxides $[Ln(OR)_3]$, and mixed amide/alkoxides "$Ln(OR)[N(SiMe_3)_2]_2$". The $Ln[SiMe_3)_2]_3$ was the favored amide due to the ease it can be metastasized. Since the amides have already been explored with limited success, the two other ligand sets (*i.e.*, alkoxides and amide/alkoxides) were studied in terms of CO_2 insertion.[24] However, background information on each of these species is detailed below.

1.4.1 Amides

Rad'kov and co-workers in 1986 synthesized a series of trisamido lanthanides $\{Ln[N(SiMe_3)_2]_n$, where Ln = Pr, Nd, Sm, Eu, Yb; n = 2, 3$\}$ and investigated their reactivities with CO_2. [24] Since the products were not crystalline, they were only identified using FT-IR spectroscopy. These investigations revealed that the metal-

containing product was contaminated with a number of secondary products, including isocyanate (Me_3SiNCO), siloxane [($Me_3Si)_2O$], and bis(trimethylsilyl)carbodiimide ($Me_3SiN=C=NSiMe_3$) species. Recently, CO_2 insertion of $Ce[N(SiMe_3)_2]_3$ was studied under an argon atmosphere at 150°C and found to yield an amorphous compound identified as "$Ce_4[N(SiMe_3)_2]_{12}(CO_2)_7$." [25] This could only be characterized by FT-IR and elemental analysis since it was not a crystalline product. In the previous research, isolation of crystal structures to accurately understand the products could not be realized for these particular amides but other $Ln-NR_2$ CO_2 insertion structures were obtained as discussed in Chapter 2. Hence, the investigation of CO_2 insertion in $Ln[N(SiMe_3)_2]_3$ was not performed for this study but was instead use as precursors for subsequent conversion to $Ln(OR)_3$.

1.4.2 Alkoxides

To study CO_2 insertions into Ln-O bonds of alkoxides, a well-characterized, structurally similar series of identically-ligated $Ln(OR)_3$ species was required. Amide/alcoholysis has proven to be the most effective and versatile route for the production of $Ln(OR)_3$ compounds *if* the $Ln(NR_2)_3$ precursor is free of alkali metal salt contamination. Syntheses of the $Ln[N(SiMe_3)_2]_3$ precursors were undertaken according to known literature procedures by reacting lanthanide halides (LnX_3) with potassium bistrimetylsilylamide [$KN(SiMe_3)_2$] (**eq 1**). The exchange with alcohols (**eq 2**) usually proceeds rapidly and can be done in variety of organic solvents at low temperature and was therefore used to synthesize $Ln(OR)_3$.

$$\textbf{LnX}_3 + 3\ \textbf{KN(SiMe}_3)_2 \longrightarrow \textbf{Ln[N(SiMe}_3)_2]_3 + 3\ \textbf{KX}_3 \qquad\qquad \textbf{[1]}$$

$$Ln[N(SiMe_3)_2]_3 + 3 \text{ H-OR} \longrightarrow Ln(OR)_3 + 3 \text{ H-N}(SiMe_3)_2 \qquad \qquad [2]$$
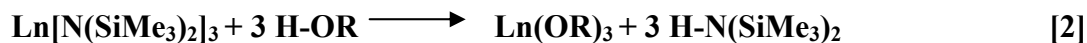
A = alkali metal (Li, K or Na); X = Br or Cl

For this study, the alcohol 2,6-di-*tert*-butylphenol (*H*-DBP) was reacted with the
appropriate amide that resulted in a three-coordinate $Ln(DBP)_3$ [Ln=Ce (**6**),[8] Sm (**7**), Dy
(**8**),[7] Yb (**9**), and Lu (**10**)] complex. This ligand was chosen due to its steric bulk that
allows for lowered coordination around the metal center, ease of crystallization, and the
formation of monomeric species across the Ln series. Monomeric species were of
interest to keep the possible variables to a minimum during the insertion reactions.
Increasing the nuclearity of the molecule could itself affect the insertion outcome. A
similar distorted trigonal planar arrangement of **6 – 10** allowed for the exploration of
cation size effects on the reactivity of CO_2 with $Ln(OR)_3$.

1.4.3 Mixed Amide/Alkoxides

Further investigation of the selectivity of CO_2 insertion into Ln-N or Ln-O bonds
concentrated on synthesis of mixed amide/alkoxide precursors (**eq 3**). However, upon
isolation, the precursors phase-separated into what appears to be the thermodynamically-
stable homoleptic products [*i.e.*, $Ln(NR_2)_3$ and $Ln(DBP)_3$]. Therefore, to avoid this
problem, this compound was generated *in-situ* and subsequent reaction with CO_2 was
then undertaken.

$$Ln[N(SiMe_3)_2]_3 + n \text{ H-DBP} \longrightarrow Ln[N(SiMe)_3]_2(DBP) + \text{H-N}(SiMe_3)_2 \qquad [3]$$

$$n = 1$$

1.5   *Summary*

The focus of this thesis is to develop the fundamental understanding of CO_2 insertion compounds as it relates to the cation size of the $Ln(OR)_3$. The previous work done on these systems is described in Chapter 2 (*vide infra*). To achieve the stated goal, a series of structurally-similar $Ln(OR)_3$ precursors that insert CO_2 and yield crystalline products is necessary.   The syntheses and characterizations of $Ln[N(SiMe_3)_2]_3$, $Ln(DBP)_3$, "$Ln[N(SiMe_3)_2]_2(DBP)$," and the subsequent CO_2 insertion products are described in detail in Chapter 3. It was expected that CO_2 would readily and fully insert into the Ln-O bonds. The selection of a system that will yield crystallographically characterizable species to unequivocal identify the final products is very important.   In addition, it was of interest to isolate mixed/amide alkoxides for CO_2 insertion. This is a very challenging problem, since -$N(SiMe_3)_2$ is known to be a good leaving group.[26, 27] Therefore, alternative routes to study CO_2 insertion into heteroleptic ligated species needs to be developed. Discussion of the reasoning behind the various ligand selection and processing conditions employed is presented in Chapter 4. It is anticipated that the extent of which CO_2 is able to insert into the Ln-O bonds of these specific compounds can be determined to further define this reactivity. Chapter 4 also presents the possible future directions that can be pursued based on the results obtained from this study.

2. Review of Related Literature

2.1 *CO₂ Insertion*

The study of CO_2 insertion into M-E [M (transition metal); E (element) = H, N, O, C, P, S, another M] bonds has been studied for many years.[1-3] Due to the abundance of CO_2 in the atmosphere, many research efforts focusing on chemical sequestration of carbon are underway.[2, 3, 14, 15, 28, 29] However, the bounty of CO_2 also poses a problem for ceramic materials processing, causing formation of carbonate intermediates as a result of CO_2 insertion into M-E bonds as previously described.[10-12] The mechanisms by which CO_2 inserts into these bonds and the binding motifs have been thoroughly reported in the literature for transition metals and are relatively well-understood.[1-3]

As a ligand, CO_2 is unique in that it has both nucleophilic and electrophilic bonding sites, allowing for a wide range of coordination complexes from reaction with metal species. The characterization of the final product is extremely important, especially utilizing single crystal X-ray diffraction, for the elucidation of CO_2 bonding motifs present in the final structures. In combination with other analytical characterization methods such as multinuclear magnetic resonance (NMR), elemental analysis (EA), Fourier transform infra-red spectroscopy (FT-IR), and melting point temperature determinations (mp), to name a few, characterizing the final products can be done with high confidence.

2.1.1 CO_2 Insertion in M-NR₂ (M = Transition or Main Group Metals)

CO_2 insertion into M-NR₂ (where R = C and M = transition or main group metal) to yield carbamates have been well-reported in the literature.[13-15, 30-38] There are two

common reaction routes used to synthesize these compounds: i) reaction of anhydrous

metal halides (MX_y) with a variety of amines (HNR_2) in the presence of CO_2, or ii)

reaction of $M(NR_2)_x$ with CO_2 vapors from dry ice or CO_2 bubbled into the reaction.[3] A

few representative metal carbamates [$M(O_2CNR_2)_y$] obtained using the first synthetic

route include group IV transition metals carbamates, $M(O_2CNR_2)_4$ (where M = Ti, Zr, or

Hf; R = Et or Pr^i), group V carbamates [$M(O_2CNR_2)_n$] (where M = Nb or Ta, R = Et, n =

5; M = Nb, R = Et, Pr^i, n = 4), and group VI carbamates [$M_2(O_2CNEt_2)_4$] (where M = Cr

or Mo).[39,30,40] In addition, several main group complexes such as $Sn[O_2CN(Pr^i)_2]_4$ and

$Al_2[O_2CN(Pr^i)_2]_6$ were obtained using this route. [38-41] Representative examples of

$M(O_2CNR_2)_y$ complexes synthesized using the second route include group 14 and 15

complexes $Sn(O_2CNR_2)_4$ (where R = Et) and $Sb(O_2CNR_2)_3$ (where R = Me, Et, Pr^i).[34] In

addition, transition metal Ti and Cr carbamates have been obtained by the reaction of

stoichiometric amounts of CO_2 with the appropriate $M(NR_2)_x$ precursor.[32,33] For group 2

cations, $Mg_6(Et_2NCO_2)_{12}$ was obtained from the addition of CO_2 to a solution of

$Mg(NEt_2)_2$.[37] However, this same compound was also formed by reacting

dibutylmagnesium with diethylamine followed by carboxylation using CO_2.[31] As in the

previous synthesis, a $Li(O_2CNR_2)$ complex was prepared by reaction of lithium alkyl

(^nBuLi) with an amine (2,3-dimethylindole) in the presence of CO_2.[35] Therefore, a third,

less-common reaction route for main group metal carbamates can be described as the

reaction of metal alkyls with amines in the presence of CO_2.

2.1.2 CO$_2$ Insertion into M-OR Bonds (M = Transition or Main group)

There are many examples of CO_2 insertions into transition metal alkoxide M-OR

bonds. [1-3, 13, 42-45] The most common routes to form these $M(O_2COR)_y$ are by i) alkoxide

uptake of atmospheric CO_2 by exposure to air, ii) *in-situ* synthesis of the appropriate

precursor complex using an alcohol and CO_2,[13, 42-44] iii) coupling CO_2 with epoxides in

the presence of metal alkyls,[45] iv) fixation of CO_2 through hydroxo metal complexes, or

v) from reaction of an alkoxide with CO_2 *via* dry ice vapors or gas cylinders. These

routes are described in detail for a wide range of transition metal carbonates. Those have

been crystallographically characterized include Ni,[46, 47] Co,[47, 48] Cu,[49] Fe,[47] Zn,[47] Zr,[50]

V,[51] Ta,[52] Ti,[53] Mo,[54] Cd,[55] W,[56-59] Mn,[47, 60] Pt,[45] Cr,[61] and Re.[60] Further discussion of

these compounds can be found in the reviews of CO_2 insertion into M-O bonds by Palmer

et al. (1983), Behr (1988) and Yin *et al.*(1999).[1-3] However, there has been only one

crystallographically-characterized compound for CO_2 insertion into main group M-OR

bonds.[62] In that report the reaction of $[M(OR)_2]_n$ polymers (where M = Mg or Ca; R =

Me or Et) with excess CO_2 to yield what appeared to be mixed alkoxide/carbonate

complexes, $[M(O_2COR)(OR)(ROH)_x]_n$. The products were characterized by NMR, FT-

IR, and TGA/DSC; however, single crystals of the products could not be achieved for

further characterization.[62] In addition $[Mg(OR)_2]_n$ (where R = Pr^i or Bu^t) polymers

dissolved in the parent alcohols were reacted with CO_2 to yield similar mixed

alkoxide/carbonate complexes. Re-crystallization of $Mg[O_2COMe(OMe)(MeOH)_{1.5}]_n$ in

a non-anhydrous solvent mixture did yield a crystalline product,

$[Mg_9(CO_3)(O_2COMe)_8(OMe)_8 (MeOH)_{13}]\cdot MeOH\cdot C_7H_8$ supporting that the former

compounds might contain mixed alkoxide/carbonato ligands.[62]

2.2 *CO₂ Insertion in Lanthanide Complexes*

As noted above, there are numerous examples of CO_2 insertion into transition

metal and main group amide and $M(OR)_x$ bonds. These yield carbamato or carbonato

ligands and the bonding motifs have been studied *via* single crystal X-ray diffraction.[63] In comparison, the investigation of insertion into Ln-NR or Ln-OR bonds is underdeveloped. This may be due to the cost of pure Ln starting materials, the lack of commercially available precursors, or the challenging syntheses required to yield pure $Ln(NR_2)_3$ starting materials.[4-6, 64-70]

2.2.1 CO₂ Insertion into Ln-N Bonds of Amides

Studies concerning the insertion of CO_2 into a variety of different Ln-N bonds for a series of $-NR_2$ compounds have been reported in the literature.[24, 71-78] The first report focused on $Ln[N(SiMe_3)_2]_3$ but the characterization of the product and by-products were limited to infra-red spectroscopy.[24] FT-IR data indicated that the CO_2 does insert, eliminating a portion of the amide as an isocyanate and other organic reaction by-products. However, a definitive understanding of the structural aspects of the metal component was not reported. Following this initial report, an extensive study involving insertion products of a series of $LnX_3(solv)_x$ (where X = halide, solv = toluene, tetrahydrofuran or dimethoxyethane) reacted with HNR_2 (where R = Pr^i, Bu, or Et) in the presence of CO_2 was reported.[71-76] The resulting products formed were carbamates (O_2CNR_2), in which the CO_2 has inserted into the M-N bond of the amide. This was shown by single crystal X-ray diffraction and FT-IR spectroscopy. In these reports a series of alkyl amides based on the *N, N'*-dialkylcarbamato lanthanide complexes $[Ln_4(O_2CNR_2)_{12}]$ (where Ln = Ce, Pr, Nd, Sm, Eu, Gd, Ho, Er, Yb, Lu, R = Pr^i; Ln = Nd, Eu, Gd, R = Bu; Ln = Nd, R = Et) were synthesized and characterized.[71-76] The series of compounds adopted the same structure but possessed different unit cell parameters (*i.e.*, isotypical). The bonding motifs for the carbamates are represented in **Figure 3**.

Figure 3. <u>mononuclear:</u> **a)** chelate η^2; <u>dinuclear:</u> **b)** bridge μ_2-η^2; **c)** chelate/bridge μ_2-η^3; <u>trinuclear:</u> **d)** bridge μ_3-η^3; <u>tetranuclear:</u> **e)** bridge μ_4-η^4.
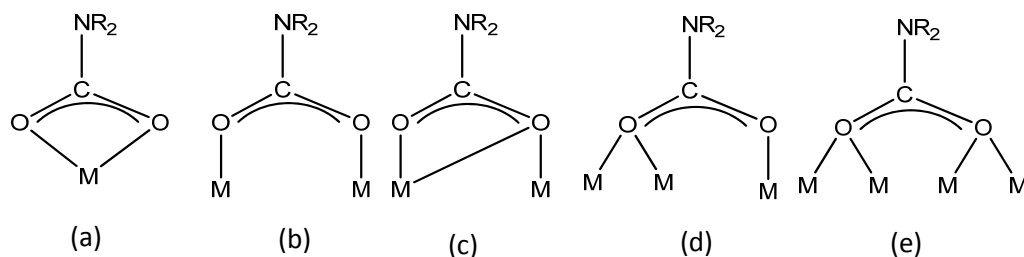
Interestingly, only the Ce carbamate derivatives contained the bonding motifs shown in (c) and (e).[73] The unique behavior was attributed to the size of the Ce atomic radii in comparison to the other *N, N'*-dialkylcarbamato Ln complexes reported.

Evans *et al.* synthesized a similar *N,N'*-diphenyl-2-carboxyhydrazino samarium complex by CO_2 insertion into the precursor $[(C_5Me_5)_2Sm]_2(\mu\text{-}\eta^2\text{:}\eta^1\text{-}N_2\text{-}Ph_2)$ which uses a diamine and *not* an amide.[79] The resulting complex was an organometallic dimeric complex crystallographically characterized as $[Sm_2(C_5Me_5)_4(THF)\{\mu\text{-}\eta_2\text{-}:\eta_1\text{-}NN(CO_2)Ph_2\}]$ (**Figure 4**).

Figure 4. $[Sm_2(C_5Me_5)_4(THF)\{\mu\text{-}\eta_2\text{-}:\eta_1\text{-}N,N'(CO_2)Ph_2\}]$.[79]
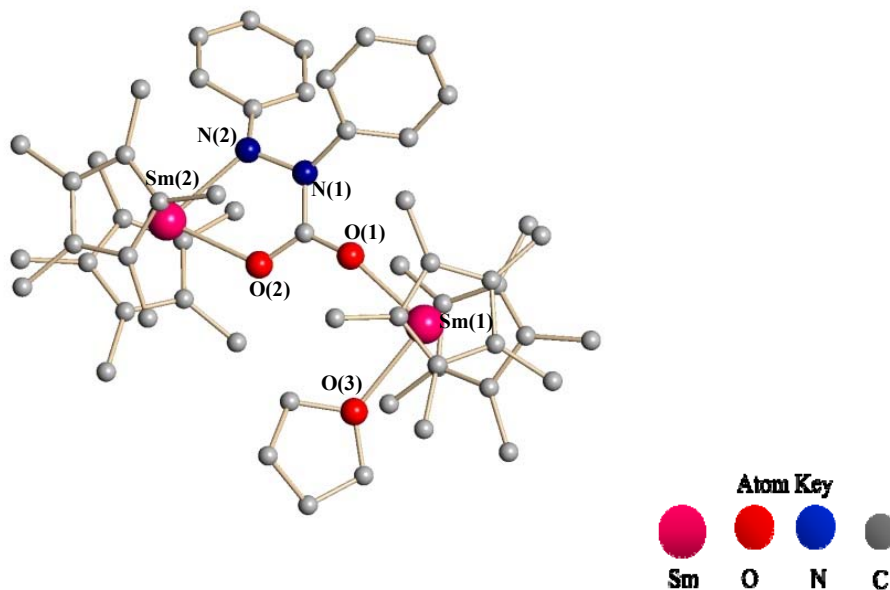
The dimeric product obtained versus the tetranuclear cluster observed in the alkylamide example most likely resulted from the sterically-hindering cyclopentadienyl (Cp* or C_5Me_5) ligands along with the diamine, thus preventing oligomerization.

It is also noteworthy that several Cp* lanthanide derivatives have been synthesized and studied for CO_2 insertion into various Ln-N or Ln-C bonds, or to give dimerization of CO_2 to yield an oxalate.[78-80] For instance, Evans *et al*. reported on the crystallographically-characterized organo-yttrium carbamate $[(C_5Me_5)_2Y(\mu\text{-}O_2CNC_6H_{10}O)]_2$ (**Figure 5**), synthesized from the CO_2 insertion into the Y-N bond of their novel ϵ-caprolactam derivative, $(C_5Me_5)_2Y(NC_6H_{10}O)$.[78]

Figure 5. [Cp$_2$Ln(η^2-O$_2$C(CH$_2$)$_3$NMe$_2$].[78]
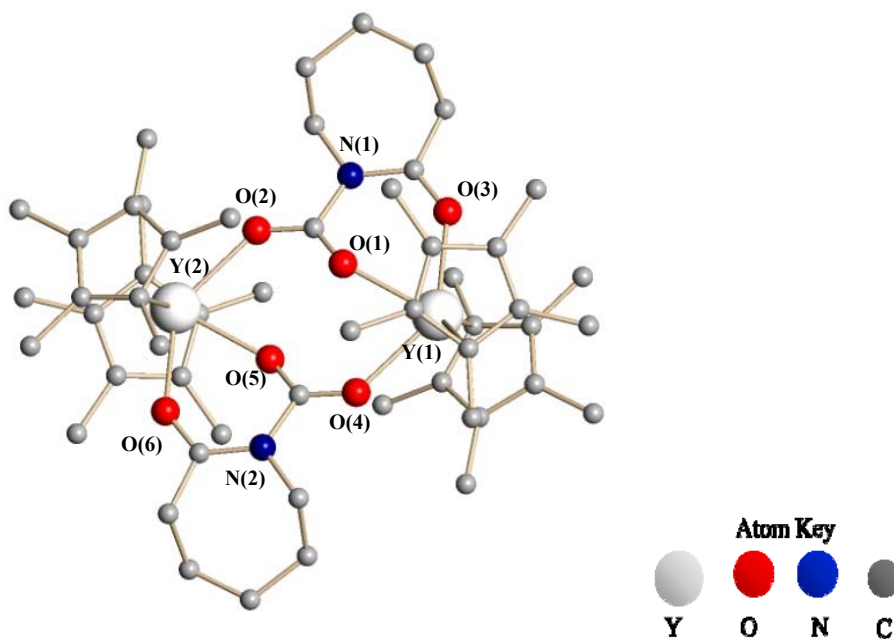
The ε-caprolactam binds in a chelating fashion through the N of the ring and the O of the alkoxide but the CO$_2$ inserts only into the Y-N bond, forming a carbamate. In comparison, CO$_2$ reactions with (Cp)$_2$Ln[NMe$_2$(CH$_2$)$_3$] (Ln = Lu, Y) were found to preferentially insert into the Ln-CH$_2$ bond of the chelating amide to break the Ln-N bond and yield [Cp$_2$Y(η^2-O$_2$C(CH$_2$)$_3$NMe$_2$]$_2$ (**Figure 6**).[77] It was shown from this work that CO$_2$ insertion favors Ln-C bonds over Ln-N bonds and Ln-N bonds over Ln-O bonds when different bond Ln-E bonds are present in the same compound.

Figure 6. $[Cp_2Y(\eta^2\text{-}O_2C(CH_2)_3NMe_2]_2$.

Atom Key

Y	O	N	C
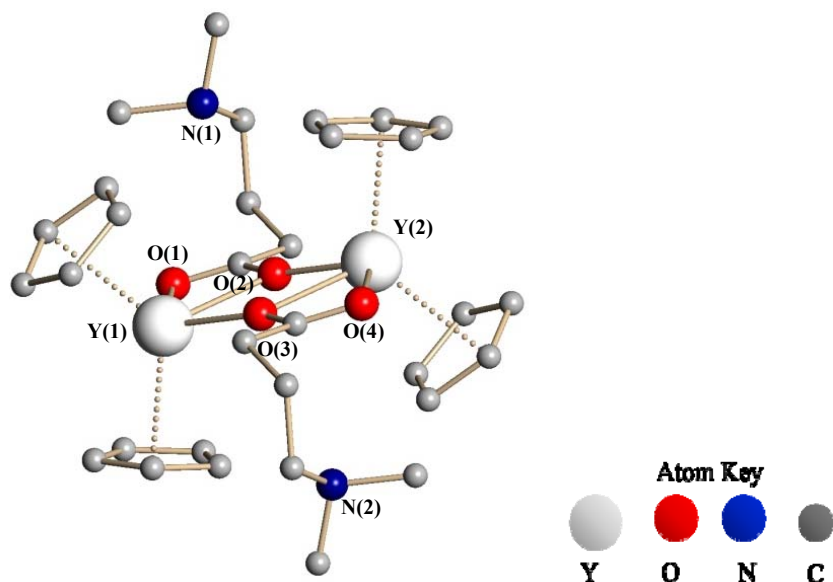
2.2.2 CO$_2$ Insertion into Ln-O Bonds of Alkoxides

There has been only one report of CO_2 insertion into a Ln-O bond of a Ln(OR)$_3$ reported by Bochkarev *et al.*[21] The "supposed" precursor was monomeric "Ln(OBu^t)$_3$" (Ln = Pr, Nd, Sm) .[21] Three equivalents of CO_2 was added in hopes of forming Ln(O$_2$COBu^t)$_3$ and infra-red spectroscopy confirmed the presence of a CO_2 stretch (1580 cm^{-1}) in the product. However, since that time, crystal structures of "Ln(OBu^t)$_3$" revealed that these species are not monomeric; rather trimeric species [Ln$_3$(μ_3-OBu^t)$_2$(μ_2-OBu^t)$_3$(OBu^t)$_4$(HOBu^t)$_2$] (where Ln = Ce or Dy) or [La$_3$(μ_3-HOBu^t)$_2$(μ_2-OBu^t)$_3$(OBu^t)$_6$] with a coordinated *tert*-butanol, a tetrameric complex [Ce$_4$(μ_3-OBu^t)$_3$(μ-OBu^t)$_4$(OBu^t)$_5$], or pentameric species [Ln$_5$(μ_5-O)(μ_3-OBu^t)$_4$(μ_2-OBu^t)$_4$(OBu^t)$_5$] (where Ln = La, Nd) with a bridging oxo ligand were actually present.[7, 81-84] Therefore, understanding the final structure of CO_2 insertion into these alkoxides was compromised due to the erroneously-

characterized starting materials. A recent review on Ln(OR)$_3$ species highlights the under use of these precursors by revealing the many alkoxide precursor voids for some of the lanthanides along the series.[85] Developing a fully-characterized library of Ln(OR)$_3$ compounds from across the series permits systematic CO_2 insertion reactions studies to be done and understood.

3. Experimental

All compounds were handled under an inert atmosphere using standard glovebox and Schlenk techniques, unless otherwise indicated. All solvents were used as received from Aldrich, obtained in Sure/Seal^{TM} bottles and handled only under an inert atmosphere of argon. The following compounds were stored under argon upon receipt from Aldrich and used without further purification: $CeBr_3$, $SmCl_3$, $DyCl_3$, $YbCl_3$ $LuCl_3$, H-DBP, and $KN(SiMe_3)_2$.

Characterization: X-ray data collections were performed on a Bruker AXS diffractometer. Crystals were transferred to a pool of Flurolube^{TM} on a glass slide and then placed under a microscope. A single crystal was then mounted onto a glass fiber of the goniometer head and placed under a stream of liquid N_2 at -100 °C for data collection.

FT-IR spectroscopic data were obtained using KBr pressed pellets using a Bruker Vector 22 Instrument under an atmosphere of flowing nitrogen. Under an inert atmosphere of Ar, crystals of each compound were mixed with KBr in a morter with a pestle until a uniform consistency was achieved. The powder was loaded into the pellet press to yield a transparent pellet of the sample. To avoid reaction with atmosphere the pellet/pellet-press were sealed in a baggie then loaded into the $N_2(g)$ filled chamber of the analyzer.

Elemental analyses were performed on a Perkin-Elmer 2400 CHN-S/O elemental analyzer. Pre-weighed aluminum ampules were loaded into the inert atmosphere glovebox and ~2.5 mg of crystalline sample was loaded separately in the ampule and then sealed. To avoid reaction with the atmosphere, the sample was placed in a vial with a

screw cap and then taken to the analyzer for final weight calculation and loaded into the instrument chamber.

Solution state ^{13}C $\{^1H\}$ NMR spectra for all compounds were obtained using a 5 mm BB solution probe on a Bruker AMX 400 MHz spectrometer. All spectra were referenced using deuterated toluene-d_8. Samples were made up in a glovebox using crystalline material and the sample tubes were flame sealed under vacuum to avoid reaction with the atmosphere.

Melting point determinations (mp) were performed on sealed samples using an Electrotherm® Melting Point Apparatus. Samples were prepared inside a glovebox by loading the powder into glass ampules that were sealed using vacuum grease before removal from the glovebox.

3.1 Amide Synthesis and Characterization

The syntheses for all $Ln[N(SiMe_3)_2]_3$ were undertaken according to reported procedures (**eq 1**).[4-6, 65, 67] Due to the similarity of synthesis procedure, a general preparative route to $Ln[N(SiMe_3)_2]_3$ is described with specific details for a particular cation, supplied below. On a Schlenk line under flowing argon, the appropriate LnX_3 was added by transfer-tube over a 1 hr period to a stirring solution of $KN(SiMe_3)_2$ in THF previously cooled to 0ºC for 30 min in an ice water bath. (*Note:* this reaction can be very exothermic so cooling the solution is necessary to control heat evolution). After complete addition of the LnX_3, the reaction mixture was stirred over night and allowed to slowly warm to room temperature. After 12 hr, the reaction mixture was removed from the bath and a liquid nitrogen side-trap connected. Volatile components were removed by

vacuum distillation to yield a brown (Sm, Ce) or off-white (Dy, Yb, Lu) powder. This powder was re-dissolved in hexanes and carefully transferred to centrifuge tubes. The mother liquor was separated from the KX by centrifugation yielding a transparent liquid. This was dried by vacuum distillation to obtain a brown (Ce, Sm) or off-white (Dy, Yb, Ly) powder. Each powder was separately loaded into a sublimator inside the glovebox, was carefully transferred to the Schlenk line and placed under vacuum (~10^{-3} torr). An acetone/dry ice mixture was placed in the cold finger of the apparatus and sublimation was performed for each $Ln[N(SiMe_3)_2]_3$ at ~150 ºC. For each sample crystals were obtained on the cold finger and used for all further characterization.

Ce[N(SiMe₃)₂]₃ (1).[5] Used $CeBr_3$ (5.00 g, 13.2 mmol), $KN(SiMe_3)_2$ (7.85 g, 39.5 mmol) and ~300 mL of THF. Yield 3.54 g (43.4%). FT-IR (KBr, cm^{-1}): 2957(s), 1252(s), 1184(s), 1012(m), 936(m), 8449s), 755(m), 678(m, sh), 657(s), 609(s). $^{13}C\{^1H\}$ NMR (100.5 MHz, C_7D_8) δ 2.58 [$N(SiCH_3)_3$]. mp 149-153 ºC.[5, 86]

Sm[N(SiMe₃)₂]₃ (2).[65] Used $SmCl_3$ (5.00 g, 19.5 mmol), $KN(SiMe_3)_2$ (11.6 g, 58.4 mmol) and ~300 mL of THF. Yield 6.50 g (52.9%). FT-IR (KBr, cm^{-1}): 2954(s), 2897(m), 2473(w), 1248(s), 1188(s), 988(m), 937(s), 829(m), 767(m), 677(s), 658(s), 603(s). $^{13}C\{^1H\}$ NMR (100.5 MHz, C_7D_8) δ 2.58 [$N(SiCH_3)_3$]. mp 154-159 ºC. [86, 87]

Dy[N(SiMe₃)₂]₃ (2).[67] Used $DyCl_3$ (5.00 g, 18.6 mmol), $KN(SiMe_3)_2$ (11.1 g, 55.9 mmol) and ~300 mL of THF. Yield 7.80 g (58.6%). FT-IR (KBr, cm^{-1}): 2958(s), 2900(m), 2362(w), 1240(s), 1187(s), 978(s), 939(s), 832(m), 771(s), 7549s,sh), 677(m), 658(m), 606(s). $^{13}C\{^1H\}$ NMR (100.5 MHz, C_7D_8) δ 2.60 [$N(SiCH_3)_3$]. mp 161-165 ºC.

Yb[N(SiMe₃)₂]₃ (4).[4] Used YbCl₃ (5.00 g, 17.9 mmol), KN(SiMe₃)₂ (10.7 g, 53.8 mmol) and ~300 mL of THF. Yield 3.54 g (30.3%). FT-IR (KBr, cm⁻¹): 2959(s), 1258(s), 11879s), 974(m), 837(m), 846(m), 773(m), 676(s), 610(s). ¹³C{¹H} NMR (100.5 MHz, C₇D₈) δ 2.54 [N(SiCH₃)₃]. mp 163-165 ºC. [86, 87]

Lu[N(SiMe₃)₂]₃ (5).[6] Used LuCl₃ (5.00 g, 17.8 mmol), KN(SiMe₃)₂ (10.6 g, 53.3 mmol) and ~300 mL of THF. Yield 5.60 g (48.1%). FT-IR (KBr, cm⁻¹): 2955(s), 2362(w), 1250(s), 1186(s), 972(s), 936(s), 833(m), 776(s), 754(s, sh), 668(s), 617(s). ¹³C{¹H} NMR (100.5 MHz, C₇D₈) δ 2.574 [N(SiCH₃)₃]. mp 167-170 ºC.[86, 87]

3.2 Alkoxide Synthesis and Characterization

A general synthesis will be described, since the preparation of all the Ln(DBP)₃ compounds were identical (**eq 2**). The appropriate amount of Ln[N(SiMe₃)₂]₃ was transferred to the 25 mL vial and 5 mL of toluene was added, and the mixture was stirred until dissolved. The appropriate amount of *H*-DBP was weighed out in a separate vial and dissolved in 5 mL toluene. That solution was added drop-wise to the stirring solution of amide. A color change occurred for each reaction, suggesting a ligand to metal charge transfer, and the color is recorded below for each specific reaction. To ensure completeness of reaction, the solution was allowed to stir for 12 hr. After this time the reaction mixture was concentrated by slow evaporation of the volatile components until X-ray quality crystals were formed.

Ce(DBP)₃ (6).[8] Used Ce[N(SiMe₃)₂]₃ (0.50 g, 0.81 mmol), H-DBP (0.58 g, 2.81 mmol) and ~10 mL of tol. Color changed from gold to dark brown. Yield 0.46 g (75.4%). FT-IR (KBr, cm⁻¹) 2958(s), 2362(m), 1425(s), 1411(s, sh), 1348(m), 1232(s), 1095(m),

862(s), 747s), 668(s), 453(w), 420(s). Elemental Analysis for $C_{42}CeH_{63}O_3$ (MW=756.08 g/mol): calc'd %C 66.72 %H 8.40. Found %C 66.31, %H 8.67. $^{13}C\{^1H\}$ NMR (100.5 MHz, C_7D_8) δ 155.9, 135.9 120.2 (C_6H_3), 34.3 [-$C(CH_3)_3$], 30.3 [-C($CH_3)_3$].

Sm(DBP)₃ (7). Used Sm[N(SiMe₃)₂]₃ (0.50 g, 0.79 mmol), H-DBP (0.57 g, 2.76 mmol) and ~10 mL of tol. Color changed from pale yellow to orange.   Yield 0.50 g (82.0%). FT-IR (KBr, cm^{-1}): 3642(m), 3079(w), 2957(m), 1583(s), 1411(s), 1386(m, sh), 1358(s, sh), 1347(s), 1244(m), 1195(s), 1143(s), 1124(s), 1098(m), 869(s), 819(s), 796(s, sh), 748(s), 658(s), 564(s), 548(s), 452(s).   Elemental Analysis $C_{42}H_{63}O_3Sm$ (MW=766.36 g/mol):   calc'd % C65.83 %H 8.29. Found C% 66.16, H% 8.34. $^{13}C\{^1H\}$ NMR (100.5 MHz, C_7D_8) δ 154.2, 135.9, 120.3 (C_6H_3), 34.3 [-$C(CH_3)_3$], 30.3 [-C($CH_3)_3$].

Dy(DBP)₃ (8).[7] Used Dy[N(SiMe₃)₂]₃ (0.50 g, 0.79 mmol), H-DBP (0.56 g, 2.71 mmol) and ~10 mL of tol. Color changed from colorless to pale yellow. Yield 0.38g (62.3%). FT-IR (KBr, cm^{-1}): 3650(m), 2958(m), 2363(w), 1458(s), 1426(m, sh), 1362(m), 1315(m), 1262(m), 1231(s, sh), 1198(m), 1143(m, sh), 1122(s), 1023(w), 867(s), 821(s), 806(m), 795(s, sh), 747(s), 691(m), 656(w). Elemental analysis $C_{42}DyH_{63}O_3$ (MW=778.46 g/mol): Calc'd C% 64.80, H% 8.16. Found C% 64.59, H% 8.32. $^{13}C\{^1H\}$ NMR (100.5 MHz, C_7D_8) δ 154.2, 135.9, 120.2 (C_6H_3), 34.3 [-$C(CH_3)_3$], 30.4 [-C($CH_3)_3$].

Yb(DBP)₃ (9). Used Yb[N(SiMe₃)₂]₃ (0.50 g, 0.77 mmol), H-DBP (0.55 g, 2.68 mmol) and ~10 mL of tol. Color changed from red to dark red/brown. Yield 0.54 g (89.4%). FT-IR (KBr, cm^{-1}): 3648 (m), 2951 (m), 2362 (w), 1457(s), 1246(s), 1361(m), 1315(m), 1250(w), 1231(m, sh), 1198(m), 1143(s), 1122(m), 1023(w), 868(m), 844(m), 821(s, sh),

806(m), 795(m), 747(s), 667(m), 588(m), 446(m), 419(s). Elemental analysis

$C_{42}H_{63}O_3Yb$ (MW=789.00 g/mol): calc'd C% 63.94 H% 8.05. Found %C 63.76, %H

8.52. $^{13}C\{^1H\}$ NMR (100.5 MHz, C_7D_8) δ 154.3, 135.8, 120.3 (C_6H_3), 34.3 [$-C(CH_3)_3$],

30.4 [$-C(CH_3)_3$].

Lu(DBP)₃ (10). Used Lu[N(SiMe₃)₂]₃ (0.50 g, 0.76 mmol), H-DBP (0.55 g, 2.67 mmol)

and ~10 mL of tol. Changed from pale yellow to light purple.   Yield 0.39 g (64.6%).

FT-IR (KBr, cm⁻¹): 3645(m), 3081(w, sh), 2957(m), 1457(m), 1425(m), 1388(s, sh),

1360(s, sh), 1316(s, sh), 1250(m, sh), 1231(s), 1196(s, sh), 1143(s), 1122(s), 1095(s,

sh), 1023(m), 878(s), 844(m), 821(m), 806(s, sh), 795(s), 746(s), 667(m), 588(m),

527(m), 449(m), 419(m).   Elemental analysis $C_{42}H_{63}LuO_3$ (MW=790.93g/mol): calc'd

%C 63.78, %H 8.03. Found %C 64.21, %H 7.98. $^{13}C\{^1H\}$ NMR (100.5 MHz, C_7D_8) δ

154.2, 135.8, 120.3 (C_6H_3), 35.0 [$-C(CH_3)_3$], 30.4 [$-C(CH_3)_3$].

3.3 *Mixed Amide/Alkoxide Synthesis and Characterization*

Attempts to isolate mixed amide/alkoxide precursors {Ln(DBP)[N(SiMe₃)₂]₂}

were abandoned due to ligand redistribution in solution to yield Ln[N(SiMe₃)₂]₃ and

Ln(DBP)₃. Upon isolation in the solid-state, crystals of each component were identified

by single crystal X-ray diffraction. The Ln[N(SiMe₃)₂]₃ crystals were thin needles and

the Ln(DBP)₃ crystals were cubes. Stoichiometric solution mixtures were chosen for all

subsequent studies.

3.4 *CO₂ Insertion Process and Characterization of Products*

A 53 mM solution of the appropriate precursor (**6** - **10)** dissolved in toluene was

put into a two-neck round bottom reaction flask and that was equipped with a nitrogen

adaptor and a rubber septum (**Figure 7**). The flask containing the solution was carefully transferred from the glovebox to the Schlenk line and placed under an Ar atmosphere. An oil bubbler was used to ensure a positive pressure of gas was maintained in the flask. Technical grade carbon dioxide (5 psig) was purged through tubing equipped with a syringe needle for two minutes to clean the line of air and yield a positive pressure of CO_2. The needle was then stuck into the septum and the argon shut off so that the oil bubbler could monitor CO_2 flow. The solution was stirred under an atmosphere of CO_2 for 30 min. during which no color changed was observed. Some of the volatile components were removed *via* vacuum distillation and the remaining solution was transferred to the glovebox for slow evaporation crystal growth.

Figure 7. Set up for low pressure CO_2 insertion
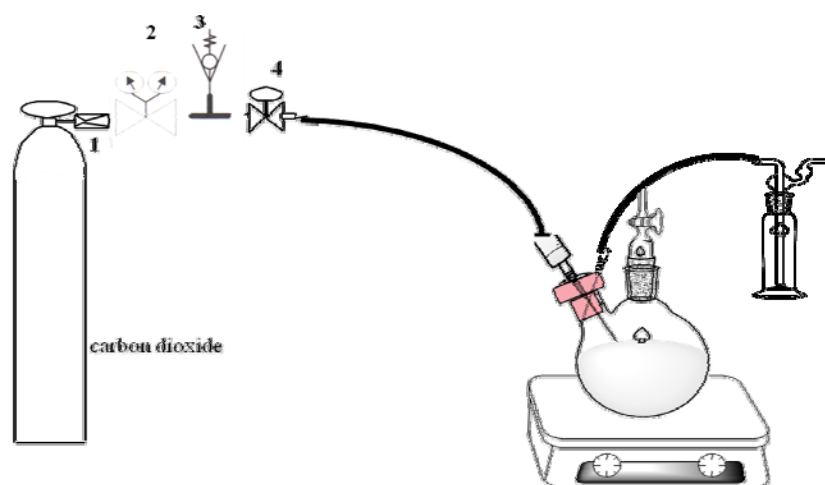
Legend

1. RFO Swagelok SS-4A-RFO-010 (0.010").
2. VWR CO_2 Regulator #55850-482.
3. Pressure relief valve – Swagelok PRV RL3S4 set at 100 psi.
4. Needle valve.

[Ce(DBP)$_2$($\mu_2\eta^3$- O$_2$C-DBP)]$_2$ (11). 53 mM solution of **6** (0.60 g, 0.79 mmol) in 15 mL toluene with 5 psig CO$_2$ for 30 min. No color change noted. Yield 0.20 g (31.8%). FT-IR (KBr, cm^{-1}) 3643(m), 2960(s), 2873(w, sh), 1625(w, sh), 1589(s), 1577(m, sh), 1482(w), 1426(s), 1411(w, sh), 1369(s), 1349(s), 1232(m, sh), 1248(s), 1195(m), 1176(m), 1143(s), 1105(s), 1039(w, sh), 1024(m), 861(s), 844(s, sh), 819(s), 807(s), 796(s), 747(s), 722(s), 676(m), 653(s), 588(m), 544(m), 450(s). Elemental analysis for C$_{86}$Ce$_2$H$_{126}$O$_{10}$ (MW=1600.18 g/mol): calc'd %C 64.55, %H 7.94; found %C 64.10, %H 8.04.

[Sm(DBP)$_2$($\mu_2\eta^2$- O$_2$C-DBP)]$_2$ •tol (12). 53 mM solution of **7** (0.61 g, 0.79 mmol) in 15 mL toluene with 5 psig CO$_2$ for 30 min. Solution changed from bright yellow to a green upon CO$_2$ addition. Yield 0.55 g (80.9%). FT-IR (KBr, cm^{-1}): 3642(m), 2962(s),1626(s), 1589(w), 1482(w), 1413(m), 1387(m), 1370(s, sh), 1347(s), 1238(m), 1188(m), 1144(s), 1115(s), 1023(m), 867(s), 844(s, sh), 820(s), 806(s, sh), 797(s), 749(s), 715(m), 569(s). 547(m), 450(m). Elemental analysis C$_{86}$H$_{126}$O$_{10}$Sm$_2$ (MW=1712.88g/mol; without toluene 1620.74g/mol): Calc'd C% 63.73, H% 7.84; Found C% 63.97, H% 7.86.

[Dy(DBP)$_2$($\mu_2\eta^2$- O$_2$C-DBP)]$_2$ •tol (13). 53 mM solution of **8** (0.62 g, 0.80 mmol) in 15 mL toluene with 5 psig CO$_2$ for 30 min. No color change noted. Yield 0.45 g (65.2%). FT-IR (KBr, cm^{-1}): 3642(m), 2961(m), 2284(w), 1619(m), 1583(s, sh), 1481(w), 1425(s). 1370(m, sh), 1348(m), 1263(m), 1231(s, sh), 1188(m), 1144(m, sh), 1117(s), 1023(w), 873(s), 844(s), 822(s), 796(s, sh), 770(s), 748(s), 694(w), 663(m), 451(w). Elemental analysis C$_{86}$H$_{126}$O$_{10}$Sm$_2$ •C$_7$H$_7$ (MW=1737.08 g/mol): Calc'd C% 64.30, H% 7.78; Found C% 64.51, H% 8.01.

[Yb(DBP)₂(μ₂η²- O₂C-DBP)]₂ (14). 53 mM solution of **9** (0.63 g, 0.80 mmol) in 15 mL toluene with 5 psig CO_2 for 30 min. No color change noted. Yield 0.42 g (62.7%). FT-IR (KBr, cm⁻¹): 3650 (m), 2961 (m), 2874(w, sh), 2347(w), 1630(s), 1585(s, sh), 1420(s), 1388(m), 1372(s),   1353(m), 1262(m), 1246(m, sh), 1187(s, sh), 1143(m), 1118(s), 1024(m), 875(s), 844(s), 822(s), 804(s), 771(s, sh), 752(s), 718(s), 665(s), 590(m), 452(s). Elemental analysis $C_{80}H_{126}O_{10}Yb_2$ (MW=1666.02 g/mol): Calc'd %C 62.00, %H 7.62; found %C 62.24 %H 7.87.

[Lu(DBP)₂(μ₂η²- O₂C-DBP)]₂ (15). 53 mM solution of **10** (0.63 g, 0.80 mmol) in 15 mL toluene with 5 psig CO_2 for 30 min. No color change noted. Yield 0.36 g (53.7%). FT-IR (KBr, cm⁻¹): 3648(m), 3082(w, sh), 2959(m), 2202(w), 1458(s), 1369(s, sh), 1349(m), 1316(s, sh), 1251(m, sh), 1230(s), 1194(s, sh), 1143(s), 1117(s), 1094(s, sh), 1023(m), 879(s), 844(m), 806(s, sh), 795(s), 746(s), 713(m), 678(m), 588(m), 446(m), 419(m). Elemental analysis for $C_{86}H_{126}Lu_2O_{10}$ (MW=1669.88 g/mol): Calc'd %C 61.86, %H 7.61; Found %C 62.41, %H 8.02.

3.5   *Elevated Pressure of CO₂ for Insertion into Ln(DBP)₃*

Compound **8** was loaded into a heavy walled glass vessel with a pop-tube adaptor equipped with a dual stage gas regular (**Figure 8**). The vessel was carefully transferred from the glovebox to a hood and a technical grade CO_2 cylinder was attached to the regulator. The stirring solution was put under CO_2 at a pressure of ~86-93 psig for 1 hr. The solution turned from colorless to dark brown. The apparatus was then evacuated *in vacuo* using a Schlenk line and then transferred back into the glovebox. The dark solution

was put into a vial and upon slow evaporation of the solvent X-ray quality crystals were

obtained. The unit cell of the crystals matched the mono-CO_2 insertion product **13**.

Figure 8. 3 oz Glass – Pressure Reaction Vessel, Andrews Glass Co.
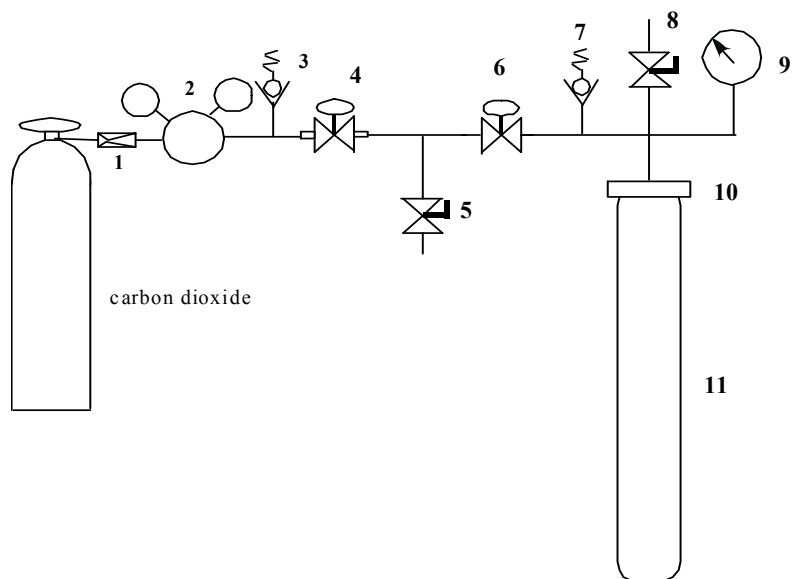
Legend

1. RFO Swagelok SS-4A-RFO-010 (0.010").
2. VWR CO_2 Regulator #55850-482.
3. Pressure relief valve – Swagelok PRV RL3S4 set at 100 psi.
4. Needle valve.
5. Swagelok valve – SS 42S4 (for vacuum evacuation).
6. Swagelok needle valve – SS-1RS4.
7. Pressure relief valve – Swagelok 4CPA2 set at 100 psi.
8. Swagelok valve – SS 42S4 (vent valve).
9. Swagelok pressure gauge 316 SS 100 psi.
10. Pressure reaction vessel head – stainless steel with o-ring and flat gasket seals, including ring couplings.
11. 3 oz, heavy walled glass reactor vessel, Andrews Glass Co.

3.6 CO₂ Insertion into Mixed Amide/Alkoxide in Solution

Since a mixed alkoxide/amide could not be isolated, the compound was generated *in-situ* and stirred for 12 hr. After this time, 5 psig pressure of CO_2 was added to the reaction mixture and left for 30 min. The majority of the volatile components were removed by vacuum distillation and the resulting solution was then set aside with the cap loose. After slow evaporation of the remaining volatile material at room temperature for 12 hr, crystals were isolated. A single X-ray quality crystal was obtained and used for characterization.

$Sm_4(\mu\text{-}CO_3)_2(\mu\text{-}O)_2(DBP)_4(THF)_2(\mu\text{-}O_2C\text{-}DBP)$ (16). Reacted **3** (0.50 g, 0.79 mmol) with 1 equivalent of *H*-DBP (0.16 g, 0.78 mmol) to produce $Sm[N(SiMe_3)_2]_2(DBP)$ *in-situ*. Yield > 1%. FT-IR (KBr,cm⁻¹) 3550(br), 2960(m), 2362(s), 2339(s), 1262(s), 1025(m), 820(w, sh), 801(m), 668(s), 457(m), 419(s).

3.7 General X-ray Crystal Structure Information

Crystals were mounted onto a glass fiber from a pool of Fluorolube™ and immediately placed in a cold N_2 vapor stream, on a Bruker AXS diffractometer equipped with a SMART 1000 CCD detector using graphite monochromatized Mo-Kα radiation (λ = 0.7107 Å). Lattice determination and data collection were carried out using SMART Version 5.054 software. Data reduction was performed using SAINTPLUS Version 6.01 software and corrected for absorption using the SADABS program within the SAINT software package. Structures were solved by direct methods that yielded the heavy atoms, along with a number of the lighter atoms or by using the PATTERSON method, which yielded the heavy atoms. Subsequent Fourier syntheses yielded the remaining light-atom

positions. The hydrogen atoms were fixed in positions of ideal geometry and refined using SHELXS software.[88-90] The final refinement of each compound included anisotropic thermal parameters for all non-hydrogen atoms. All final CIF files were checked at http://www.iucr.org/. Disorder in the metal centers for compounds **9** and **10** coupled with disorder in the *t*-butyl groups made locating several protons on the methyl groups difficult to ascertain. Therefore, several protons were omitted in the final structure solution, yet the refinement values were still in tolerance for acceptable compounds. Similar disorder was observed for compounds **14** and **15**, and these were treated under the same conditions. Compound **11** contained disorder in the terminal and bridging ligands. The SAME command was used in attempts to model this disorder however improvement on the overall structure was not observed. The disorder in the structure also forced solution to be done in a non-centrosymmetric setting. The discussion of all structure solutions including disorder within the structures are presented in detail in Chapter 4.

4. Results and Conclusions

In order to undertaken a systematic investigation of cation size effect of CO_2 insertion into Ln-O bonds, it was necessary to have a set of iso-structural $Ln(OR)_3$ complexes. The first step was to generate the amide precursors $Ln[N(SiMe_3)_2]_3$ (**eq 1**) needed for conversion into the alkoxides, $Ln(DBP)_3$ (**eq 2**), and finally to react them with CO_2. Characterization of these compounds, particularly by single crystal X-ray diffraction, proved to be critical in identifying the resulting compounds and correctly determining the bonding modes of the inserted CO_2 moiety. In addition, other analytical tools (FT-IR, EA, mp, and NMR) were used to aid in the characterization of the bulk materials. Details of the syntheses, processing, and characterization of these novel products are described below.

4.1 *Amides {Ln[N(SiMe₃)₂]₃}*

Prior to preparation of the desired $Ln(OR)_3$, it was necessary to synthesize the amide precursors $Ln[N(SiMe_3)_2]_3$. The -$N(SiMe_3)_2$ derivative in comparison to the other available -NR_2 moieties was chosen due to the simplicity of exchange with alkoxides and the relative ease of purification to remove the alkali contaminants. In addition, the synthetic routes for these amides are available in the literature for many of the lanthanides. [4-6, 64-70, 91] Therefore, each $Ln[N(SiMe_3)_2]_3$ complex was synthesized and characterized by the methods below before subsequent reactions were investigated.

4.1.1 Synthesis

A series of representative $Ln[N(SiMe_3)_2]_3$ compounds [Ln = Ce (**1**), Sm (**2**), Dy (**3**), Yb (**4**), and Lu (**5**)] were synthesized according to **eq 1**.[4-6, 65, 67] A brief description of the reaction is provided below with details supplied in Chapter 3. All of the $Ln[N(SiMe_3)_2]_3$ compounds were synthesized from the reaction of $KN(SiMe_3)_2$ in tetrahydrofuran (THF) with the appropriate LnX_3.   The K salt was ultimately decided upon since purification of the amide from this alkali metal has proved the most successful (*i.e.*, Li and Na inclusion occur more readily). The reaction was allowed to stir for 12 hr. and then the volatile components were removed by vacuum distillation. The amide was extracted with hexanes and the KX removed by centrifugation. The mother liquor was dried *via* vacuum distillation to yield an off white powder. Since purification of these amides is a crucial step to avoid alkali metal salts in subsequent reactions additional purification by sublimation was performed for each amide. For completeness, the characterization data for all the amides was included in the Experimental Section (Chapter 3).   These results are consistent with the previously reported amide compounds.[4-6, 65, 67]

4.1.2   Bulk Characterization

4.1.2.1   Analytical Evaluation of $Ln[N(SiMe_3)_2]_3$ Compounds

The number of analytical tools available to distinguish pure $Ln[N(SiMe_3)_2]_3$ species from the alkali halide contaminated material is limited. For example, the EA data collected for compounds **1** - **5** yielded inconsistent results. This was most likely a reflection of the high volatilities of the lanthanide amides, which limits their utility in the

available instrument.[86, 87] Therefore, an alternative method, melting point determination, was employed. The mp for the majority of the Ln[N(SiMe₃)]₃ were available from the literature for comparison and the mp values obtained for **1 - 2** and **4 - 5** were found to be in good agreement.[86] However, no mp had been previously reported for **3**, but the measured value fell between the mps for the adjacent Ln congeners. This indicated that pure materials were present. Further characterization by FT-IR and NMR are discussed in detail below.

4.1.2.2   FT-IR of Ln[N(SiMe₃)₂]₃ Compounds

FT-IR spectroscopy was used to characterize the functional groups for the Ln[N(SiMe₃)₂]₃ precursors. The fingerprint region of the spectrum (1500-400 cm^{-1}) contains the characteristic stretches for M-L bonds. For compounds **1 - 5** the presence of the N-R₂ stretches were observed in the range of 620-600 cm^{-1} which is agreement with literature values.[92] A strong band in between 700–590 cm^{-1} was tentatively assigned to a Ln-N bond stretch as noted by black stars in **Figure 9**.[93] In addition, the functional group region of the spectrum (*i.e.*, 4000-1500 cm^{-1}) contains the C-H stretches (3000 cm^{-1}) from the methyl groups of the amide ligands (**Figure 9**).

Figure 9. Stacked FT-IR spectra plot of **1** – **5** (where black stars indicated the Ln-N stretch).
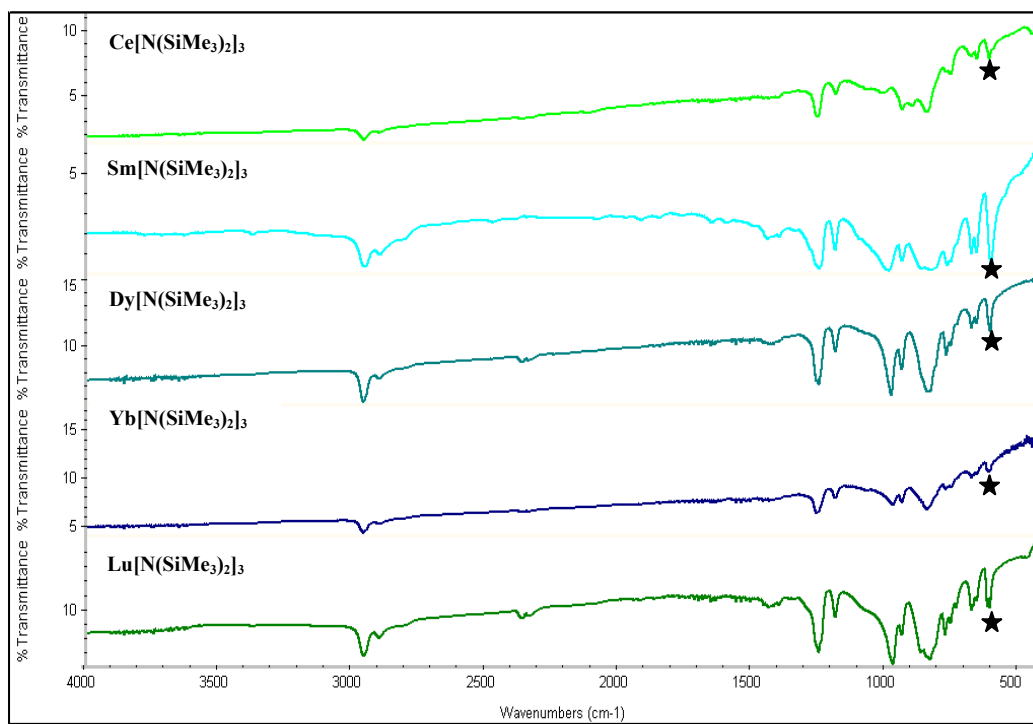
4.1.3 Crystal Structures of Ln[N(SiMe$_3$)$_2$]$_3$ Complexes

The structures of compounds **1 - 5** have been previously reported as monomeric species with the amide ligands in a distorted trigonal planar arrangement around the Ln metal center resulting in D$_3$ symmetry (**Figure 10**).[4-6, 65, 67] Additionally, there was *z*-direction disorder in the metal center above and below the plane of symmetry which required modeling that resulted in 50% partial occupancy of the two Ln atoms.[4-6, 65, 67] Herrmann *et al.* reported the deviations in the *z*-direction, as well as the bond distances and angles for most of the Ln[N(SiMe$_3$)$_2$]$_3$ compounds.[67] The unit cell parameters were used to confirm the identity of the compounds **1 - 5**. Structural solutions were obtained and the bond distances and angles as well as deviations in the metal centers for **1 – 5** were in agreement with literature reports.[4-6, 65, 67]

Figure 10. Structure plot of **2** that is representative of **1 - 5**. Thermal ellipsoids of heavy atoms are drawn at the 30% level and carbon atoms are shown as balls and sticks for clarity.
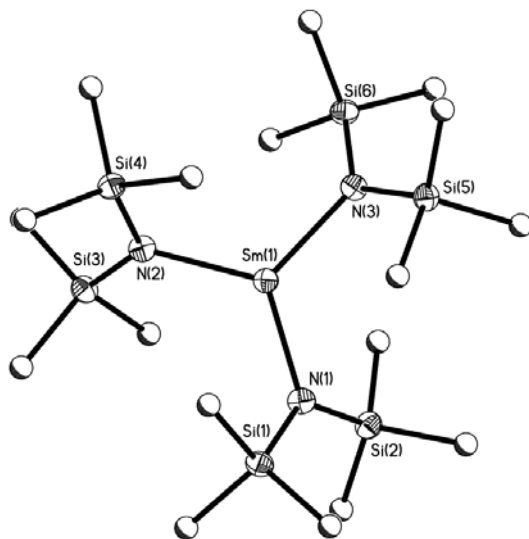
Often in these structures the metal center is close enough to the amido ligands (2.8-3.2Å) to interact with the silicon or methyl groups. Therefore, it was of interest to determine if the dislocation of the metal allows for interaction with the methyl groups of the –N(SiMe$_3$)$_2$ in an agostic interaction. It is reported that the FT-IR (*vide infra*) Ln-H-C stretches should appear in the range 2688-2692 cm^{-1}. Since no peaks were present in this area of the region for **1-5,** no agostic interactions could be assigned in these compounds.[94]

4.1.4 $^{13}C\{^1H\}$ NMR of Ln[N(SiMe$_3$)$_2$]$_3$ Compounds

Typically, ^{1}H and ^{13}C NMR data are not reported for the Ln cations due to the supposed distortion of the magnetic field by the unpaired electrons in the *f*-orbitals. While this proved true for the ^{1}H NMR data, useful information could be obtained from the ^{13}C NMR spectra (**Figure 11**). For each of the Ln[N(SiMe$_3$)$_2$]$_3$ complexes, the $^{13}C\{^1H\}$ NMR spectrum in toluene-*d$_8$* revealed a single resonance for the methyl carbons of the amide group, and the results are tabulated in **Table 1**. The $^{13}C\{^1H\}$ shift for Ce[N(Si(Me)$_3$)$_2$]$_3$ previously reported to be δ 2.50 ppm,[68] was found to be slightly down shifted for **1**. This may be a reflection of sample concentration or the field strength of the magnet used for each the individual collection. The remainder of the chemical shifts fall within a similar range as discussed for the Ce derivative.

Figure 11. ^{13}C NMR spectrum of **1** that is representative of **1 - 5**.
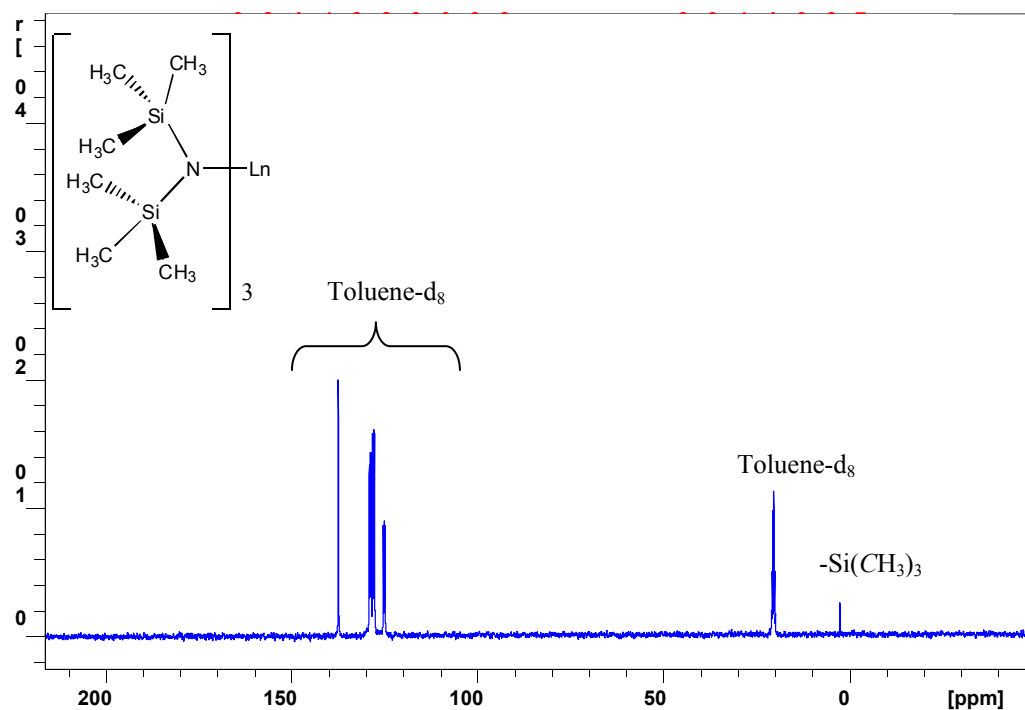
Table 1. ^{13}C NMR chemical shifts (ppm) for compounds **1 – 5**.

Compound	^{13}C{^{1}H}: Ln{N[Si(CH$_3$)$_3$]$_2$}$_3$
Ce[N(SiMe$_3$)$_2$]$_3$ **(1)**	δ 2.58 ppm
Sm[N(SiMe$_3$)$_2$]$_3$ **(2)**	δ 2.58 ppm
Dy[N(SiMe$_3$)$_2$]$_3$ **(3)**	δ 2.60 ppm
Yb[N(SiMe$_3$)$_2$]$_3$ **(4)**	δ 2.54 ppm
Lu[N(SiMe$_3$)$_2$]$_3$ **(5)**	δ 2.57 ppm

4.2 *Alkoxides [Ln(OR)₃]*

Metal alkoxides are of interest as precursors for ceramic metal oxides due to their ease of crystallization, high volatilities, commercial availability of some members, and low decomposition temperatures. Unfortunately, there are few commercially-available lanthanide alkoxides "Ln(OR)$_3$" and the compounds reported in the literature do not utilize the entire lanthanide series, thus limiting the possible precursor options. These deficiencies led to our investigation of Ln(OR)$_3$. In our recent review, a list of crystallographically characterized "Ln(OR)$_3$" that are currently available are listed by metal and ligand.[85]

4.2.1 Synthesis

The general synthesis for Ln(OR)$_3$ is shown in **eq. 2** (termed an amide alcoholysis) where the solvent can be non-coordinating (*i.e.*, hexanes or toluene) or coordinating (*i.e.*, tetrahydrofuran or pyridine). A wide range of HORs can be used to manipulate the coordination around the Ln based on the steric bulk of the ligand. For this project an aryl alcohol 2,6-di-*tert*-butanol (*H*-DBP or HOC$_6$H$_3$-2,6-C(CH$_3$)$_3$) was chosen due to ease of crystallization of the products and ability to control the final structure due to the volume the ligand takes up around the lanthanide (Tolman cone angle ~110-115°).[95] In addition, bulky ligands like DBP can avoid possible equilibrium issues between monomer/dimer that can result in more complicated products. Compound **6** and **8** were previously crystallographically-characterized in the literature and the data obtained for this report were in agreement with what was reported.[7, 8] The alkoxides were completely characterized by the methods discussed in detail below.

4.2.2 Bulk Characterization

4.2.2.1 Analytical Evaluation

Although the EA data were not useful for the amide precursors, it could be utilized for the alkoxides since they are more likely to decompose rather than volatilize or melt under the conditions employed. The elemental analyses of **6 - 10** were within the accepted 0.5% error of the calculated values for the crystalline compounds. In addition, the absence of the NR_2 and OH stretches in the FT-IR spectral analysis of **6 – 10** indicates that the amide alcohol exchange reaction has gone to completion.[92] A series of Ln-O stretches which were not present for the amides appear in the fingerprint region as indicated by black stars in **Figure 12** in the range from 590-400 cm^{-1}, again indicating that amide alcoholysis occurred.[92] A broad peak is also present around 3600 cm^{-1} that could be from residual alcohol (*H*-DBP) that was retained during sample preparation.

Figure 12. Stacked FT-IR spectra plot of **6 – 10** (where the black stars indicate Ln-O stretch)**.**
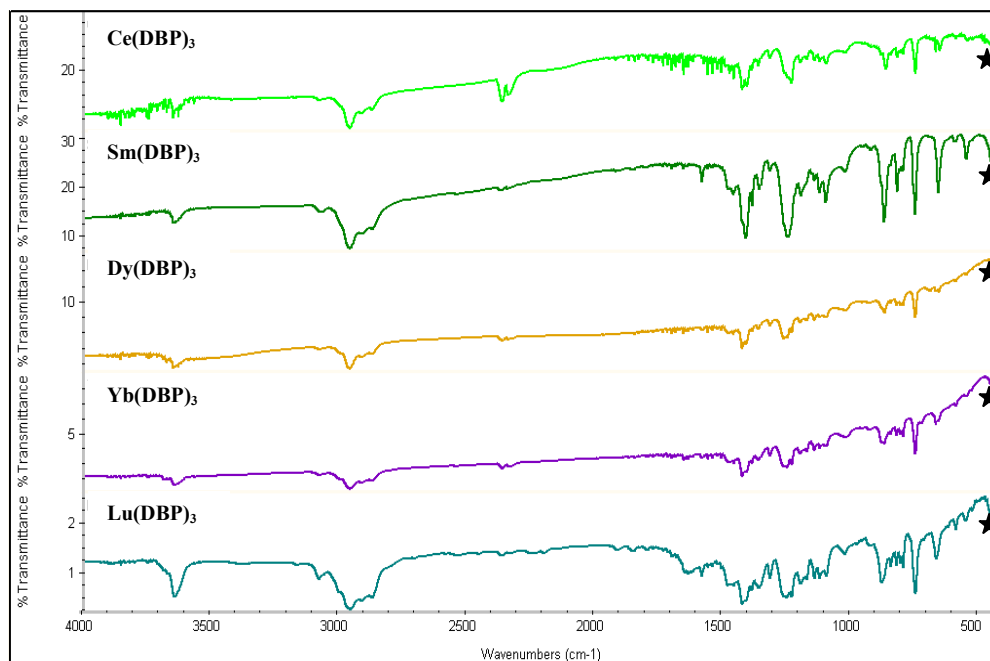
4.2.3 Crystal Structure and Metrical Data of Ln(OR)₃ Species

The crystal structures of $M(OR)_x$ often contain disorder within the atoms of the ligand chain, causing higher than normal final correlations.[96-99] Modeling disorder is a difficult process but it can be undertaken in hopes to improve the refinement values of the overall structures. Therefore, details describing each structure solution are included for clarity and justification of the disorder. Compounds **6** and **8** have been reported in literature to adopt trigonal geometries around the metal centers.[7, 8] Both compounds have disorder in the metal centers from the plane in the *z*-direction (0.54 Å and 0.58 Å, respectively). They appear to be forced into a trigonal pyramid shape due to the sterics of the ligand, not as a result of a lone pair of electrons on the metal which conventionally is

41

what trigonal pyramidal geometries require.[7, 8] However, the Ln-O bond angles for **6** and

8 are between trigonal pyramidal (109.5°) and trigonal planar (120°) due to this

distortion. In addition, neither structure appears to have an interaction between the metal

and the pendant *t*-butyl chains. The average Ln-O bond distance for **6** is 2.14 Å and for **8**

is 2.05 Å, while the average O-Ln-O bond angles are 114.15 and 112.27°, respectively,

which match the literature values. Compounds **7**, **9**, and **10** have not been previously

disseminated and were found to adopt the same trigonal geometry as the Ln(DBP)$_3$

structures reported in literature. Selected bond distances and angles are listed in **Table 4**

for these compounds and were in agreement with the Ln(DBP)$_3$ congeners previously

discussed.   Compound **7** did not have disorder in the metal center and there are two

independent molecules in the unit cell.

Figure 13. Structure plot of **9** that is representative of **6 - 10**. Thermal ellipsoids of heavy atoms are drawn at the 30% level and carbon atoms are shown as balls and sticks for clarity.
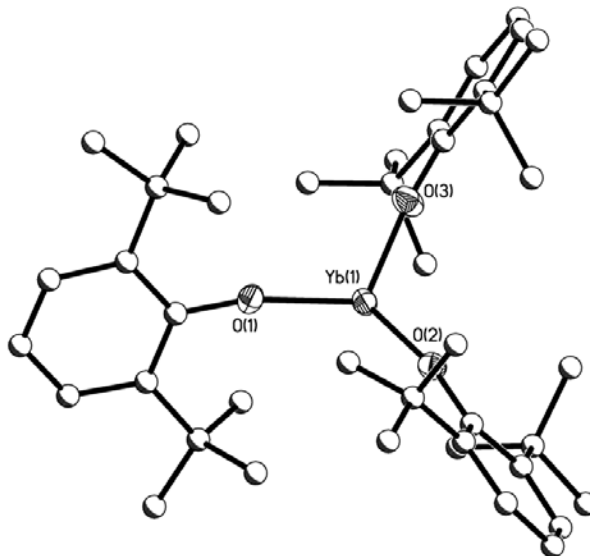
For **9** and **10**, there was disorder in the location of the Ln center with a 0.46 and 0.57Å deviation, respectively from the plane. As a result of the disorder in **9**, one of the Yb atoms is close enough to neighboring methyl group, which also has some disorder, indicate a bonding motif ($r_{(Ln-C)}$ 3.09 Å). Therefore, it was not possible to locate the hydrogen atom on that methyl group from the single crystal X-ray data because of the Ln-C interaction. One cannot tell whether agostic interactions are present or perhaps some simple disorder in the structure to cause the Ln-C bonding. As before, it was of interest to explore agostic interactions from the FT-IR data. For compounds **6, 8,** and **9** no IR peaks were found in the agostic interaction range but for **7** and **10** very weak peaks were visible in this region. However, these peaks were comparable to the noise in the spectrum, and no agostic interaction could be assigned with certainty in the absence of other characterization methods.

4.2.4 NMR of Ln(OR)$_3$ Compounds

4.2.4.1 ^{1}H NMR of Ln(OR)$_3$ Species

NMR studies in toluene-d_8 were explored to understand the solution behavior of these compounds. Even though many of the lanthanides are paramagnetic and garnering useful information from NMR can be challenging[86] ^{1}H NMR data was collected for all of the compounds but resulted in very broad resonances that were un-identifiable due to overlapping peaks. However, the ^{13}C NMR spectra led to useful information.

4.2.4.2 ^{13}C{^{1}H} NMR of Ln(OR)$_3$ Species

The ^{13}C{^{1}H} NMR spectra were obtained (**Figure 15 - Figure 18)** for compounds **6 – 10**. The expected spectrum for the three-fold symmetry (D$_3$) of the Ln(DBP)$_3$ complex was four resonances arising from the carbons of the aromatic ring appearing in the 150-120 ppm range, one resonance from the quaternary carbon, and one resonance from the methyl carbon of the *t*-butyl group that appear in the 40-30 ppm range. For **8** and **9** the expected chemical shifts are present with the methyl carbons of the *t*-butyl located at 30.4 ppm, and the quaternary C resonance is at 34.3 ppm for both compounds. The methyne carbons of the ring are present in the region of 155-118 ppm with all peaks visible except the one located at 125.0 ppm. This is due to the overlap with the toluene-d_8 reference peak, which does not permit resolution of that peak. The table below lists the resonances for the reference ligand *H*-DBP and the observed resonances for compounds **6 - 10.**

Table 2. $^{13}C\{^1H\}$ NMR chemical shifts for **6 - 10**.

Compound	δ $^{13}C\{^1H\}$: phenyl carbons[a]				$^{13}C\{^1H\}$: t-butyl carbons	
					-C(CH₃)₃	-C(CH₃)₃
H-DBP	**155.0**	**135.9**	**125.0**	**120.3**	**34.3**	**30.3**
(6) Ce(DBP)₃	**155.9**	**135.9**	-----[b]	**120.2**	37.1	32.3
					34.3	**30.3**
(7) Sm(DBP)₃	**154.2**	138.8	-----	**120.3**	36.2	31.3
		135.9		118.7	**34.3**	**30.3**
					30.2	
(8) Dy(DBP)₃	**154.2**	**135.9**	-----	**120.2**	**34.3**	**30.4**
(9) Yb(DBP)₃	**154.3**	**135.8**	-----	**120.3**	**34.3**	**30.4**
(10) Lu(DBP)₃	**154.2**	**135.8**	-----	**120.3**	**35.0**	32.2
				118.4		**30.4**

[a] $^{13}C\{^1H\}$ NMR shifts for **6 - 10**. Shifts in bold have been confirmed to be the correct assignments for each carbon by DEPT135 experiments.
[b] ----- resonances could not be separated from the tol-d_8 resonances

The $^{13}C\{^1H\}$ spectra of compounds **6**, **7**, and **10** contained additional resonances in the *t*-butyl and aromatic regions. The peaks in the aromatic region were tentatively assigned to residual non-deuterated toluene solvent in the samples. The additional peaks around the *t*-butyl region indicated by black dots in **Figure 15b, Figure 16b,** and **Figure 18b** could be attributed to several different causes: (a) perhaps a dynamic process caused by the spinning of the *t*-butyl groups; (b) an agostic interaction of the methyl groups with the Ln metal; or (c) intermolecular H-bonding interaction with neighboring *t*-butyl groups

(Figure 14). Upon inspection of the *t*-butyl groups in the solid-state structure, the

methyls are 'locked' in different positions which would yield unique NMR environments

for each methyl carbon. This suggests that all their resonances should be observable in

the ^{13}C spectrum, however; in solution, since the ligands are free to rotate, the three

methyl groups should average to a single resonance. The experimental spectra obtained

for **6**, **7**, and **10** appears to be somewhere in-between these two scenarios. Therefore, a

series of VT(variable temperature)-^{13}C{^{1}H} and DEPT135 NMR experiments were

undertaken to elucidate their solution behavior.

Figure 14. Schematic of Ln(DBP)$_3$ potential solution behavior
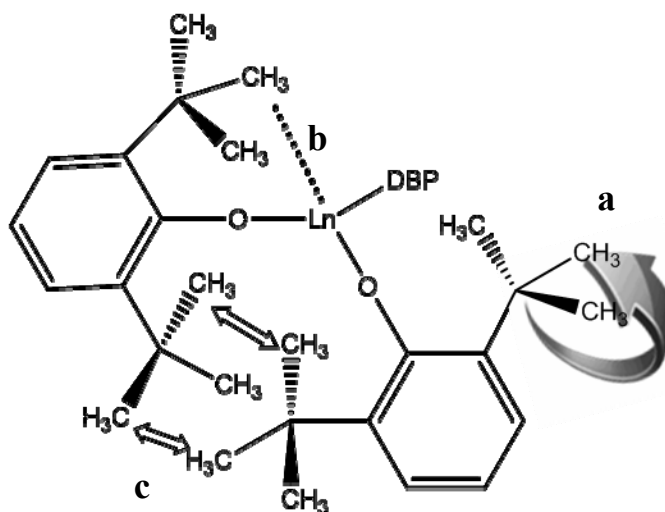
a) Rotation of the *t*-butyl groups. **b)** Methyl groups pointing toward metal led to agostic
interaction. **c)** Intermolecular interaction of neighboring *t*-butyl groups due to steric
hindrance of the ligand.

Figure 15. a) Full ^{13}C NMR spectrum for **6**. **b)** Expansion of *t*-butyl region

a)
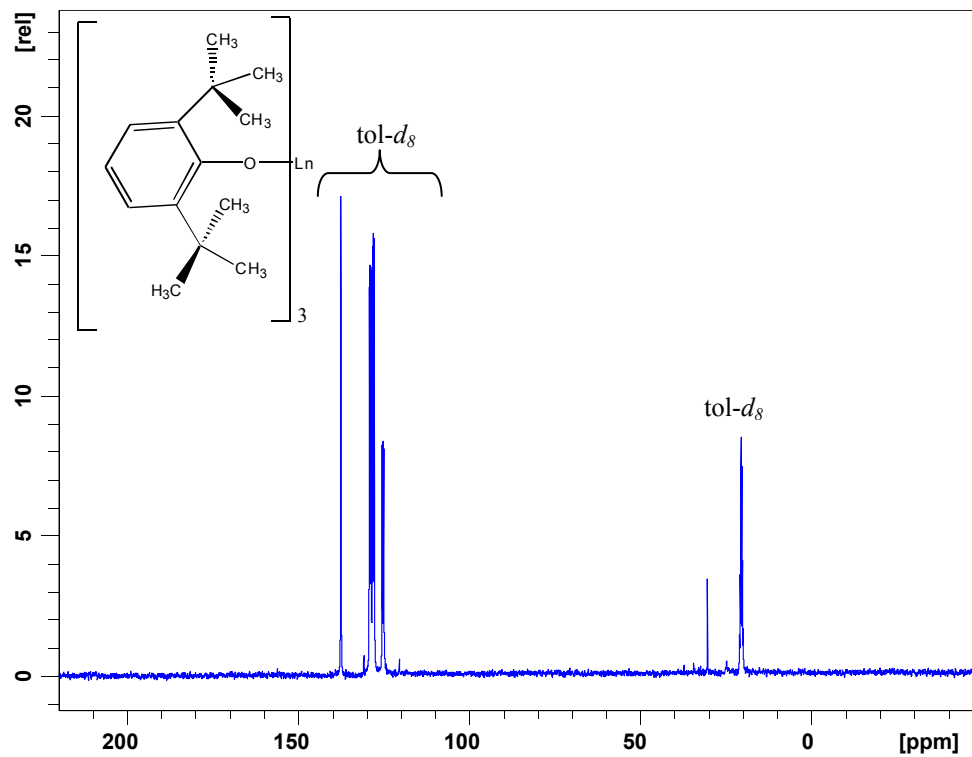
b) Black dots indicate additional peaks found in the spectrum
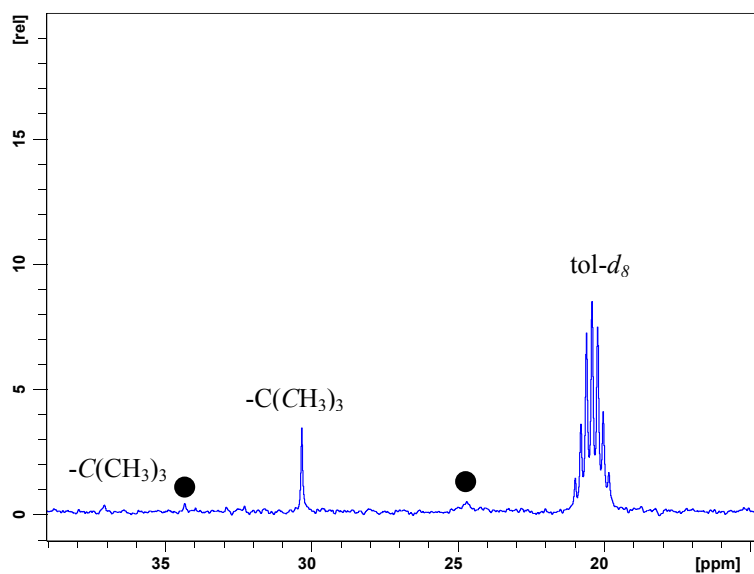
Figure 16. a) Full ^{13}C NMR spectrum for **7**. **b)** Expansion of *t*-butyl region

a)
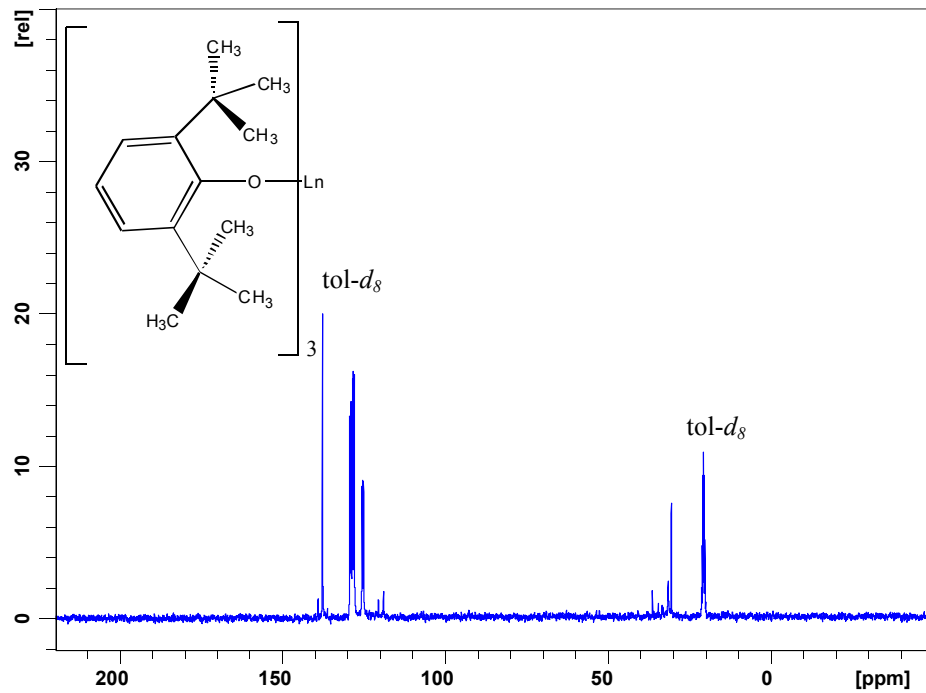
b) Black dots indicate additional peaks found in the spectrum
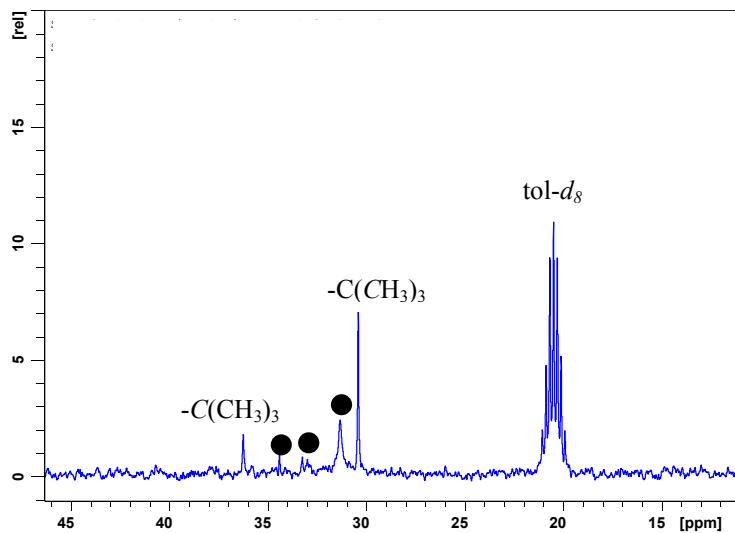
Figure 17. a) Full ^{13}C NMR spectrum for **8** that is representative for **9**. **b)** Expansion of *t*-butyl region

a)
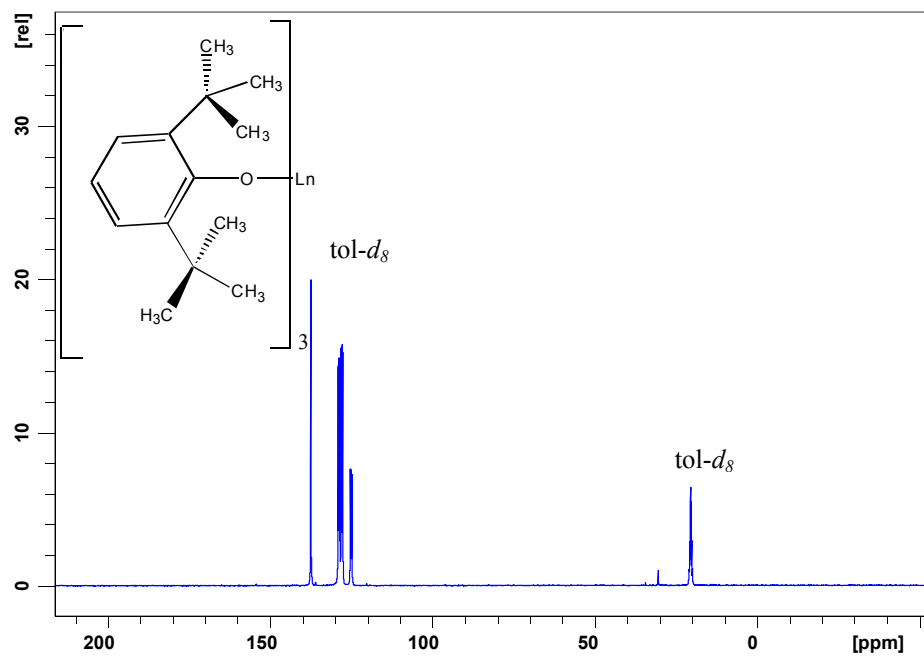
b)
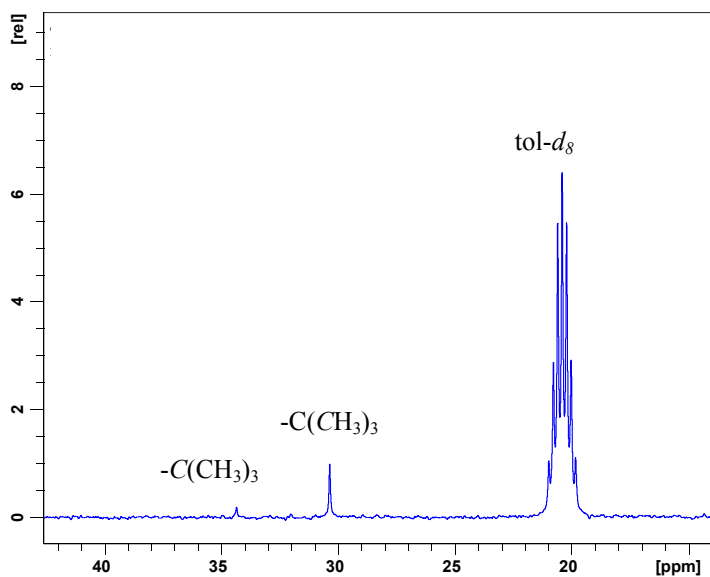
Figure 18. a) Full ^{13}C NMR spectrum for **10,** b) expansion of *t*-butyl region

a)
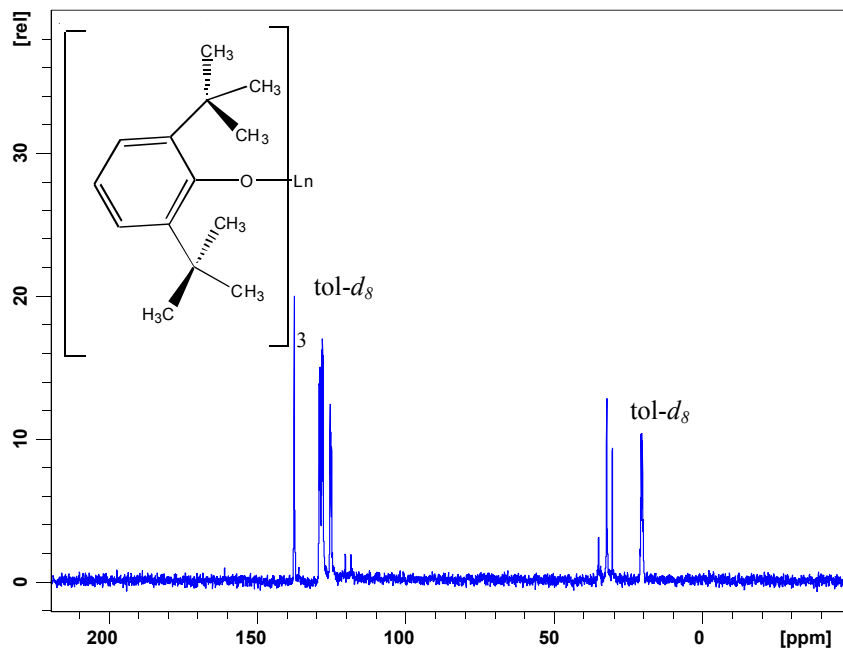
b) Black dots indicate additional peaks found in the spectrum
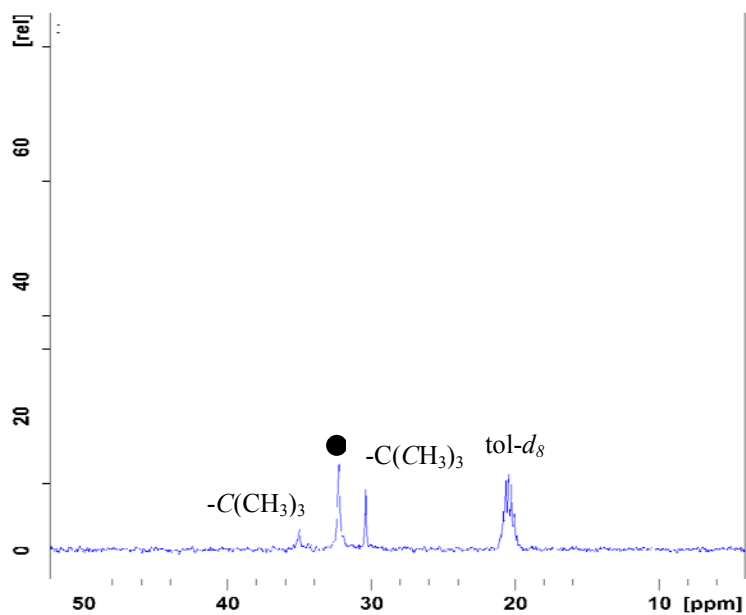
4.2.4.3 VT-^{13}C NMR of Ln(OR)$_3$ Species

VT-^{13}C NMR spectra were collected for **6**, **7**, and **10** in an attempt to identify the spurious peaks observed in the ^{13}C spectra that were not consistent with the simple solid state structure. It was expected that upon heating of these compounds the ligands should be free to rotate and a singlet should be observed for the methyl carbons. However, heating compound **6** to +60 °C resulted in a modified with to two singlets at 30.3 ppm for the *CH*$_3$ carbons and 34.3 ppm for the quaternary carbon of the *t*-butyl. Due to instrument's temperature limitations, overcoming the barrier for free ligand rotation could not be achieved. Therefore, the additional peaks in the ^{13}C NMR spectrum were assumed to be due to hindered rotation of the sterically bulky *t*-butyl group. This results in the CH$_3$ groups to experience. Alternatively, at low temperatures(-40 °C) it was expected that the ligands would lock into a single conformation, resulting in multiple methyl group resonances; however, decreasing the temperature for **6** caused preferential precipitation from solution and no useful information could be gained. This behavior was also observed in the spectrum for **7**. For compound **10** the spectrum did not vary in the high temperature range investigated. Again, the instrument limitation prevents the observed coalescence of the splitting for the methyl resonances of compounds **6**, **7**, and **10**. In addition, cooling caused the sample to precipitate out so that no information could be gained. Due to the limited information obtained from the VT-NMR data, alternative studies were needed to confirm peak identification and to determine the solution processes occurring for these samples at ambient temperature.

4.2.4.4 DEPT135 NMR of Ln(OR)₃ Species

In DEPT135 NMR experiments peaks attributed to odd number protonated carbon centers (*i.e.*, CH and CH_3) point up while peaks due to even numbered ones (*i.e.*, CH_2) point down, while quaternary carbons and deuterated solvent peaks will not be present. The expected spectrum for a Ln(DBP)₃ complex would consist of four peaks oriented up for the aromatic carbons and one peak oriented down for the methyl carbon. The DEPT135 spectra for **6 - 9** confirm the assignments for the methyl of the *t*-butyl groups [-C(CH_3)₃] resonances at 30.3 (**6**), 30.36 (**7**), 30.4 (**8**), and 30.4 ppm (**9**) as shown in **Figure 19** for spectrum of **7** that is representative of **6 - 9**.

Figure 19. DEPT135 NMR spectrum for **7** that is representative of **6 - 9**.
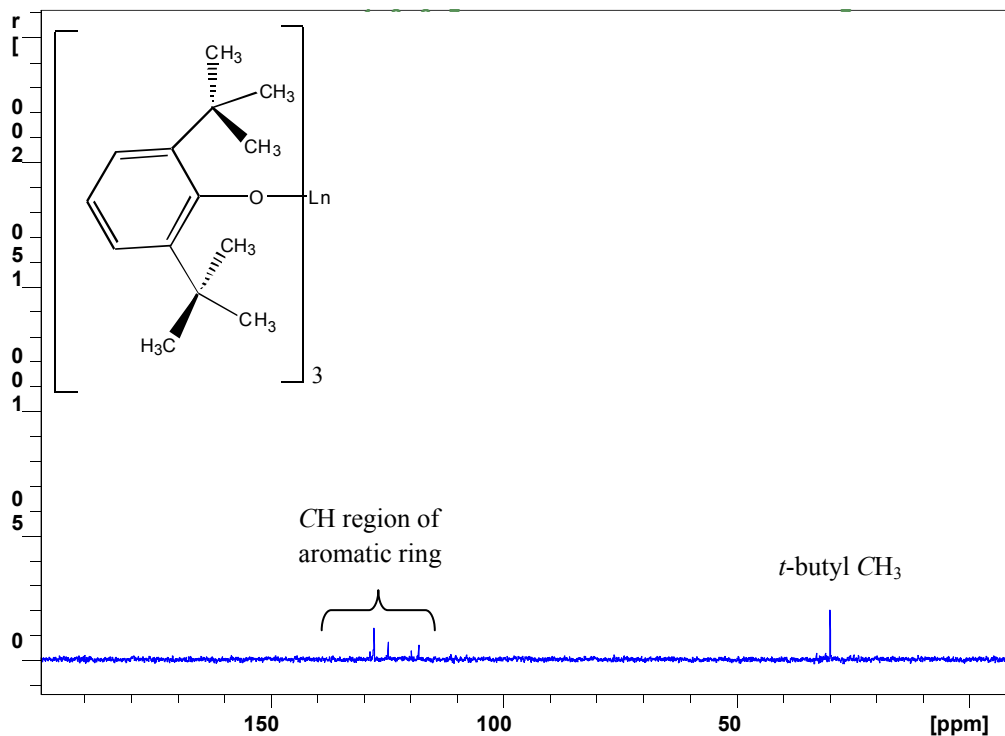
Assigning the aromatic ring resonances was complicated by their overlap with residual toluene solvent peaks. In attempts to avoid overlap with reference solvent, deuterated cyclohexane-d_{12} was used. However, the spectrum became more complex with even more sample/solvent peak overlap. Coordinating deuterated solvents were not used to ensure that no side reactions would occur. The CH_3 group on the toluene solvent was confirmed around 20.4 ppm. The additional peaks observed in the ^{13}C NMR spectra of **6** and **7** were not present in the DEPT135 spectra. Therefore, the excess peaks were attributed to the slow rotation of the *t*-butyl groups at ambient temperatures resulting in splitting. In the DEPT135 spectra for compound **10** there are two peaks in the *t*-butyl region located at 32.2 and 30.4 ppm (**Figure 20)** that are assigned to the equilibrated methyl carbons. The resonance at 30.4 ppm is in the sample range as the shift observed for compounds **6 – 9**. Further characterization by 2D ^1H-^{13}C NMR spectroscopy had to be performed on **10** to determine the correct assignment for the second peak.

Figure 20. DEPT135 NMR spectrum for **10**.
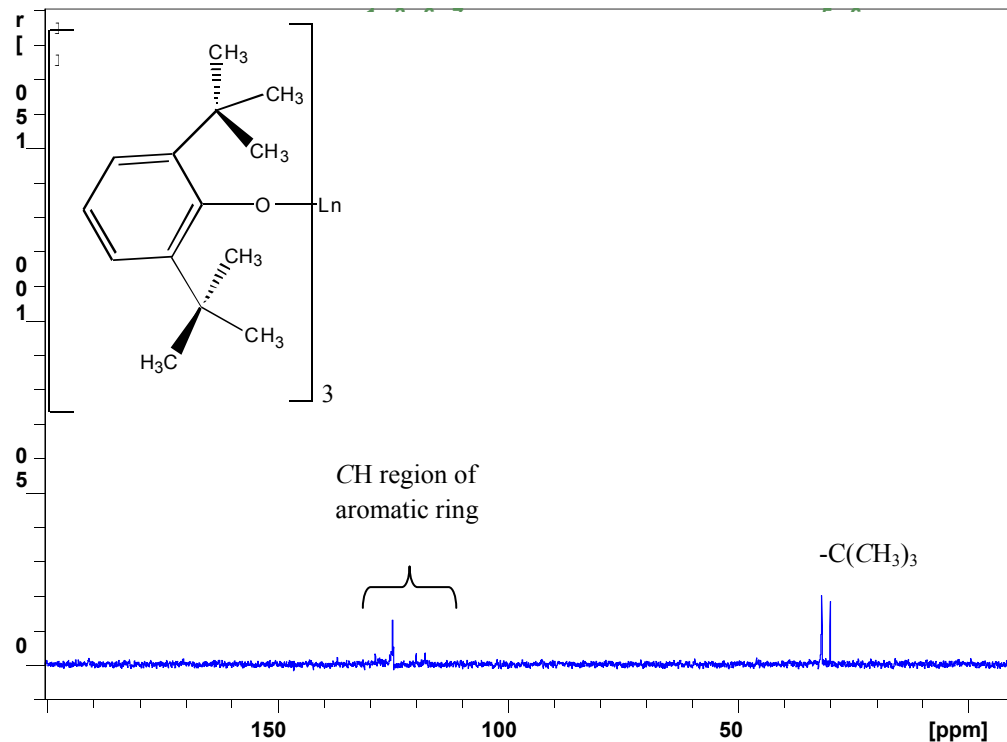
4.2.4.5 2D ^{1}H-^{13}C NMR for Compound 10

As discussed above, compound **10** has three peaks in the *t*-butyl region for the ^{13}C spectra. One of the peaks can be assigned to the quaternary C, while the other two are in a relative ratio of 3:1 (in both ^{1}H and ^{13}C spectra) with small splittings (68.2 Hz for the ^{1}H spectra and 183.9 Hz from the ^{13}C spectra). In the VT-^{13}C studies the same three peaks were present at high temperatures, while the DEPT135 spectrum had two peaks in *t*-butyl region, again with a relative ratio of 3:1. Since these results were not conclusive for peak assignment, a 2D ^{1}H-^{13}C NMR experiment was performed. The 2D experiment indicated a correlation between the splitting of the two CH_3 carbons in the ^{13}C spectra with the splitting of the CH_3 hydrogen atoms in the ^{1}H spectra (**Figure 21a** and **21b**).

54

Figure 21. **a)** 2D ^{1}H-^{13}C NMR spectrum for **10**. **b)** Expansion of splitting correlation between ^{13}C and ^{1}H.

a)

^{1}H spectra

^{13}C spectra

Splitting of *t*-butyl methyl ^{13}C peaks correlating with splitting in methyl ^{1}H peaks

toluene correlation

b)
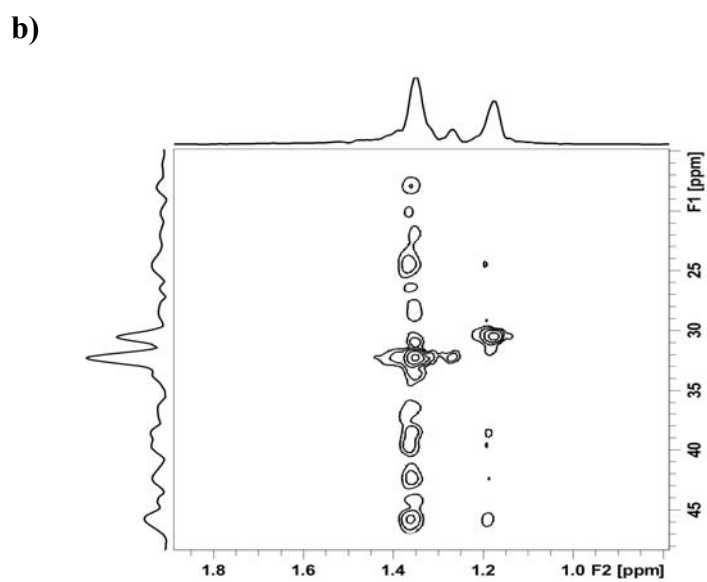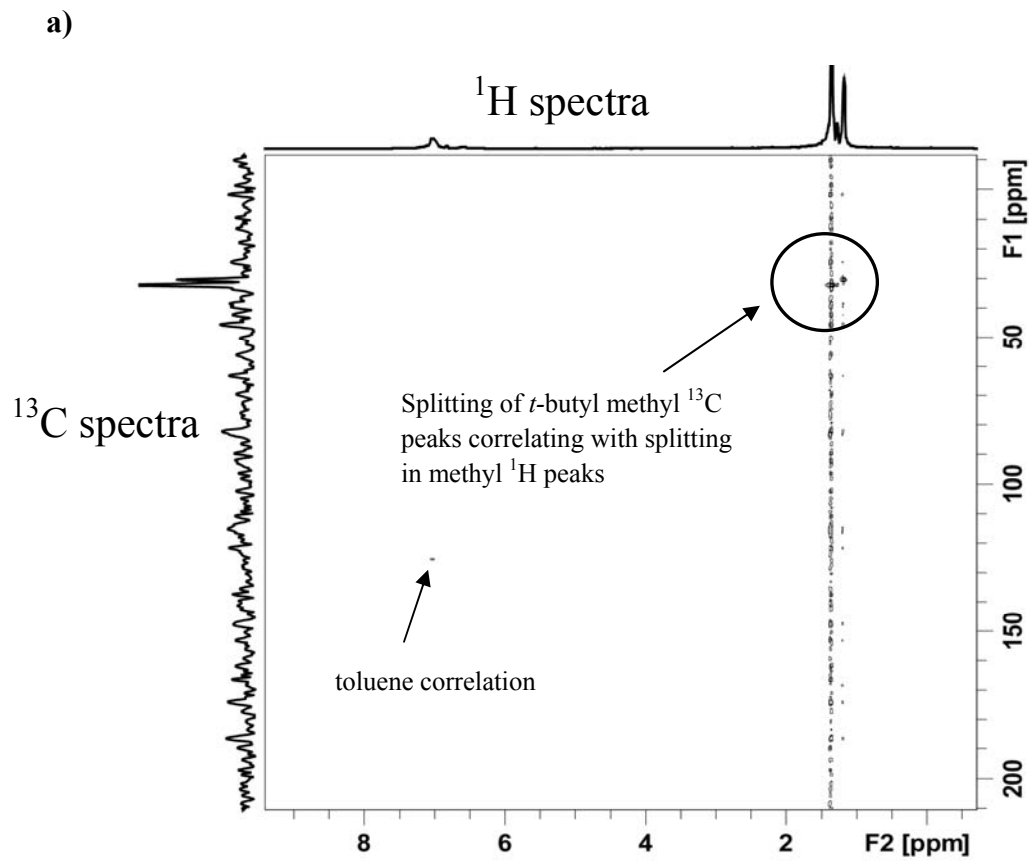
This confirms that 30% of the time the CH_3 group on the *t*-butyl is in a slightly different environment. This behavior is better described as a magnetic inequivalence, which means although the carbon of the methyl groups should be chemically equivalent by symmetry. The slow rotation of the ligand causes an individual methyl group to have a different coupling resulting in resonance splitting. In order to confirm this process, one last VT-^{1}H study was done at high temperature (60°C) to determine if heating the sample would increase the *t*-butyl rotation enough to remove the splitting. However, two peaks are observed confirming the attainable temperatures are not high enough to equilibrate the methyl groups into a single resonance (**Figure 22c** and **22d**).

Figure 22. c) ^{1}H spectrum of *t*-butyl region of **10 d)** VT-^{1}H NMR spectra of **10** showing splitting of methyl groups at high temperature (60°C).
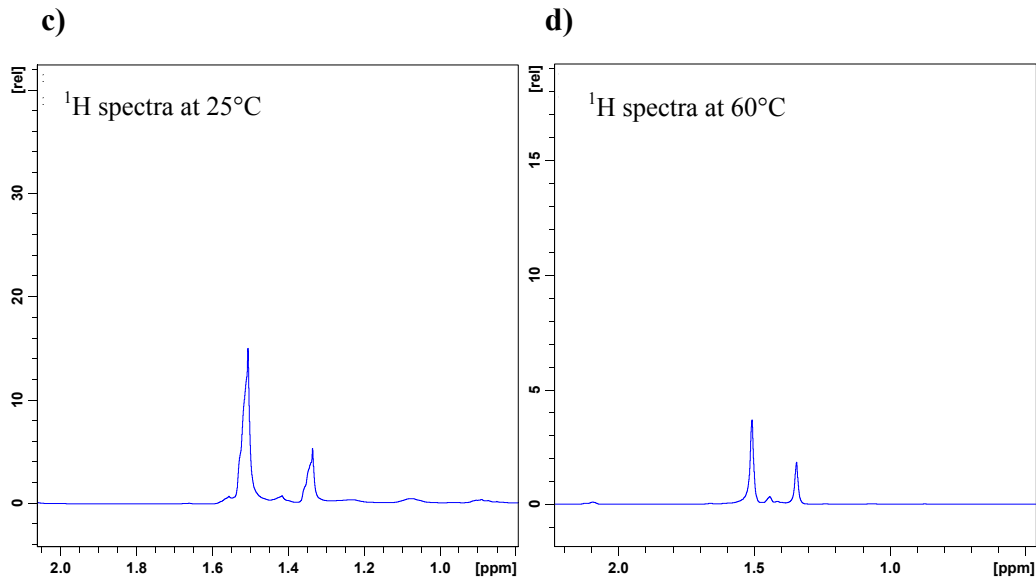
4.2.4.6 Conclusions for Solution-State Ln(OR)₃ Compounds

Because the solid-state X-ray crystal structures of compounds **6 – 10** were not

definitive in defining the Ln-ligand interaction (*i.e.,* agostic interaction or not), other

analyses were done. NMR data suggest that no agostic interactions can be assigned. The

additional peaks present were confirmed to be from steric hindrance of the ligand causing

slow rotation in solution yielding the methyl groups that could not be averaged by heat

into a single resonance.   The FT-IR data contains a very weak peak in the Ln-H-C stretch

region (2688-2692 cm^{-1}) for **7** and **10**; however, the peaks are of the same magnitude as

the noise in the spectrum, and so they were not assigned as agostic interactions. As for

the rest of the compounds (**6, 8,** and **9**) no agostic stretches are present in the IR spectra.

Therefore, the Ln-N(SiMe₃)₂ interactions in the crystal structure model was attributed to

the *z*-direction disorder in the metal centers and not agostic interactions.

4.3   Mixed Amide/Alkoxide

4.3.1   Synthesis

There are very few Ln mixed amide/alkoxide complexes reported in literature that contains the -N(SiMe$_3$)$_2$ moieties.[100-102] Reaction of compounds **1 - 5** with one or two equivalents of *H*-DBP in toluene was performed in hopes of obtaining a mixed amide/alkoxide. Upon crystallization of either mixed amide/alkoxide a) Ln(DBP)[N(SiMe$_3$)$_2$]$_2$ or b) Ln(DBP)$_2$[N(SiMe$_3$)$_2$] (Ln = Sm) two products were obtained, Ln(DBP)$_3$ and Ln[N(SiMe$_3$)$_2$]$_3$. These appear to be the thermodynamically stable product which was presumed after multiple attempts were made to isolate mixed species, always resulting in the generation of these products. Therefore, the *in-situ* generated product was undertaken. If the mixed amide/alkoxide was present then CO$_2$ insertion could be done and the subsequent product characterized.

4.3.2   NMR of Mixed Amide/Alkoxide

^{13}C NMR spectroscopy of "Sm[N(SiMe$_3$)$_2$]$_{3-n}$ (DBP)$_n$" (where *n* = 1 or 2) revealed a –N[Si(*C*H$_3$)$_3$]$_2$ fragment at 2.6 ppm and the *t*-butyl resonances at δ 30.5 and 24.5 ppm. The previous products had resonances at 2.6 ppm for Sm[N(SiMe$_3$)$_2$]$_3$ and 34.3 and 30.3 ppm for the *t*-butyl resonances of Sm(DBP)$_3$. The carbons on the aryl ring again overlapped with the toluene solvent. All final assignments were confirmed by DEPT135 NMR spectroscopy. Because of the electronegativity difference for the two ligands, the Ln-E bonds are polarized toward the more electronegative atom (O), resulting in an upfield shift as seen for the *t*-butyl carbons but an insignificant shift was observed for the

amide carbon. These results suggest that both ligands are attached to the Ln metal in solution.

4.4   CO$_2$ Insertion Products

4.4.1   General Synthesis

There are many ways to introduce CO_2 into reactions. For this research, CO_2 in gaseous form was used because of the simplicity of the experimental setup and the insertion success our group had using main group complexes.[14, 15, 29] A schematic of the experimental setup is seen in **Figure 7** and described as follow. The appropriate compound dissolved in toluene was exposed to 5 psig CO_2 for 30 min. using standard Schlenk line techniques. Half the volume of the volatile components was removed *via* vacuum distillation, increasing the concentration and promoting crystal growth. The resulting crystals were obtained by slow evaporation of the remainder of the solution and were then characterized as described below.

4.4.2   Amides CO$_2$ Insertion

As previously discussed, attempts to study CO_2 insertion of the Ln[N(SiMe$_3$)$_2$]$_3$ was not pursued for this research because of previous reports suggesting that crystalline products could not be obtained.

4.4.3   Alkoxide CO$_2$ Insertion Results

CO_2 insertion reactions were undertaken individually for compounds **6 – 10** as discussed in Chapter 3. A series of lanthanide alkoxycarbonates, **11 – 15,** were prepared. In brief, the Ln(OR)$_3$ reagent was dissolved in toluene and CO_2 bubbled through at room

temperature and pressure. The resulting compounds were identified as [Ln(μ-O$_2$C-DBP)(DBP)$_2$]$_2$ by single crystal X-ray diffraction (**Figure 24 – Figure 28**) and characterized by the following methods.

4.4.3.1 Bulk Characterization of [Ln(μ-O$_2$C-DBP)(DBP)$_2$]$_2$ Species

4.4.3.1.1 Analytical Evaluation

The elemental analyses of **11 - 15** were within the acceptable 0.5% error of the calculated values for the crystalline compounds. For compound **12**, one toluene molecule had to be removed from the calculation. The lack of solvent can be attributed to drying the crystals by vacuum distillation prior to analysis. FT-IR analyses indicated that a carbonato functional group, (O$_2$COR), was present as shown by a sharp band in the range of 1640-1620 cm^{-1}. If the ligand was bridging as for **11 – 16** (**Figure 24 – Figure 28**), or chelating as noted for compound **11** (**Figure 24**), a second weaker CO vibrational band in the range of 1355-1335 cm^{-1} would be present.[49, 92, 103, 104] The O$_2$COR peaks were observed for **11** at 1630, **12** at 1626, **13** at 1619, **14** at 1630, and **15** at 1636 cm^{-1}, respectively as indicated by black triangles in **Figure 23**. In addition, weaker bands were also present as indicated by black starts in the figure for **11** at 1346, **12** at 1347, **13** at 1348, **14** at 1353, and **15** at 1349 cm^{-1}, respectively, which suggest the bonding modes of the carbonato groups are bridging or chelating. This structural feature was confirmed in the single crystal X-ray structures. In addition a broad peak is present around 3600 cm^{-1} which is attributed to residual alcohol (*H*-DBP) present during sample preparation.

Figure 23. Stacked FT-IR spectra plot of **11 – 15** (where the O_2COR peaks are indicated by black triangles and stars).
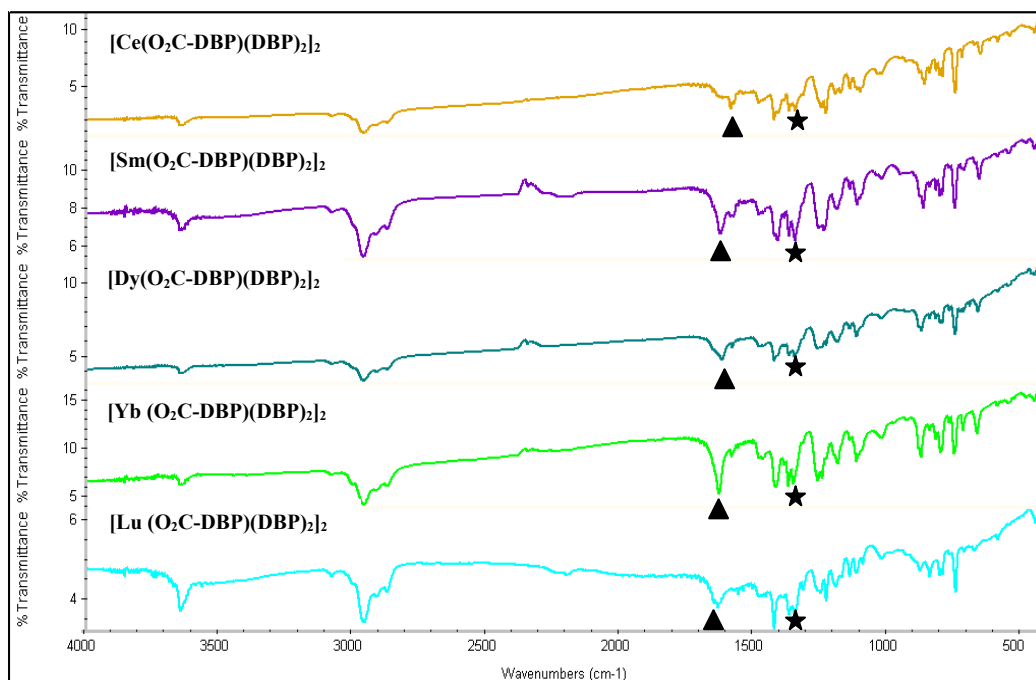
4.4.3.2 Crystal Structures and Metrical Data of [Ln(μ-O₂C-DBP)(DBP)₂]₂ Complexes

Single crystal X-ray diffraction provided the best insight as a model of the compounds in crystalline form. Compound **11** solved as a dimer with each Ce atom being 5-coordinate, adopting a distorted trigonal bipyramidal geometry that resembles more of a distorted t-shape configuration due to the $\mu_2\eta^3$-O₂C-DBP ligand (**Figure 24**). The geometry is dictated by the chelating/bridging ligand, which causes some rigidity in the final conformation. There was disorder in the DBP groups resulting in larger than normal thermal parameters and a slightly higher refinement value. Disorder within the atoms of

the pendant hydrocarbon chain is not uncommon for alkoxides due the flexibility of the ligand, resulting in higher final correlations than is typically observed for structure solutions.[96-99, 105, 106] All attempts to crystallize higher quality products were not successful, with disorder noted for each solution. Compound **11** was the optimal structure finalized. The disorder removed symmetry in the molecule and required the structure to be solved in a non-centrosymmetric setting, P1. In attempts to resolve the disorder the SAME command within the SHELX software package was used to unify the bond distances and angles in the ligands. After all the modeling, the refinement value did not improve, so further attempts were abandoned when it was determined that R1 and R2 were within acceptable tolerance values for disordered alkoxides. Additionally, one of the *t*-butyl groups had significant disorder and locations of the hydrogen atoms were not possible. Despite the disorder a reasonable refinement value was obtained and the unique bonding motif for the carbonate ligand proved to be in agreement with what has been reported in the literature for a similar Ce carbamate compound.[73]

Figure 24. Structure plot of **11**. Thermal ellipsoids of heavy atoms are drawn at the 30% level and carbon atoms are shown as balls and sticks for clarity. *Note*: disorder in the ligands caused abnormal thermo-parameters for the oxygen and carbons therefore these were excluded for clarity.
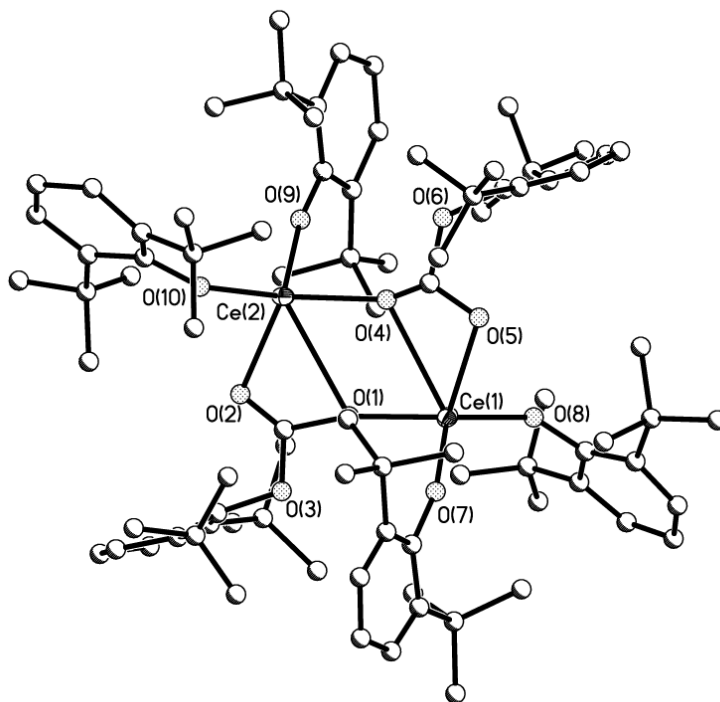
Compounds **12-15** were found to solve in the same general dinuclear arrangement with one bridging $\mu_2\eta^2$-O_2C-DBP ligands and two terminal DBP ligands for each Ln. Each metal center is 4-coordinate with the ligands arranged in trigonal bipyramidal (tbp) geometry (**Figure 25 – Figure 28**)

Figure 25. Structure plot of **12**. Thermal ellipsoids of heavy atoms are drawn at the 30% level and carbon atoms are shown as balls and sticks for clarity.
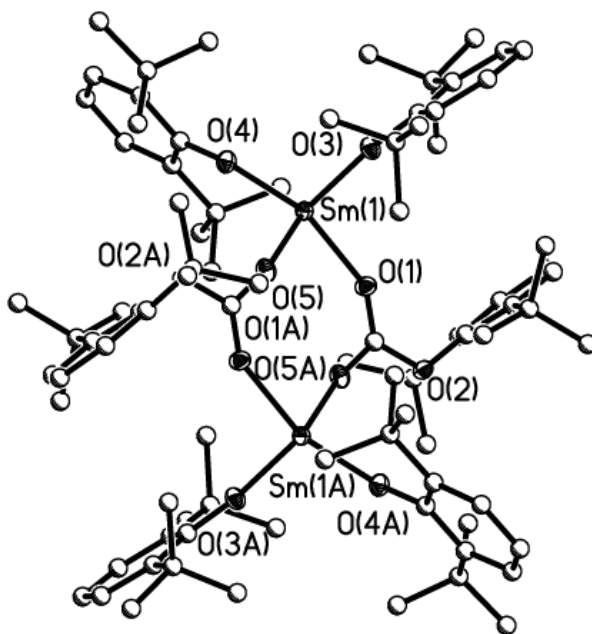
Figure 26. Structure plot of **13**. Thermal ellipsoids of heavy atoms are drawn at the 30% level and carbon atoms are shown as balls and sticks for clarity.
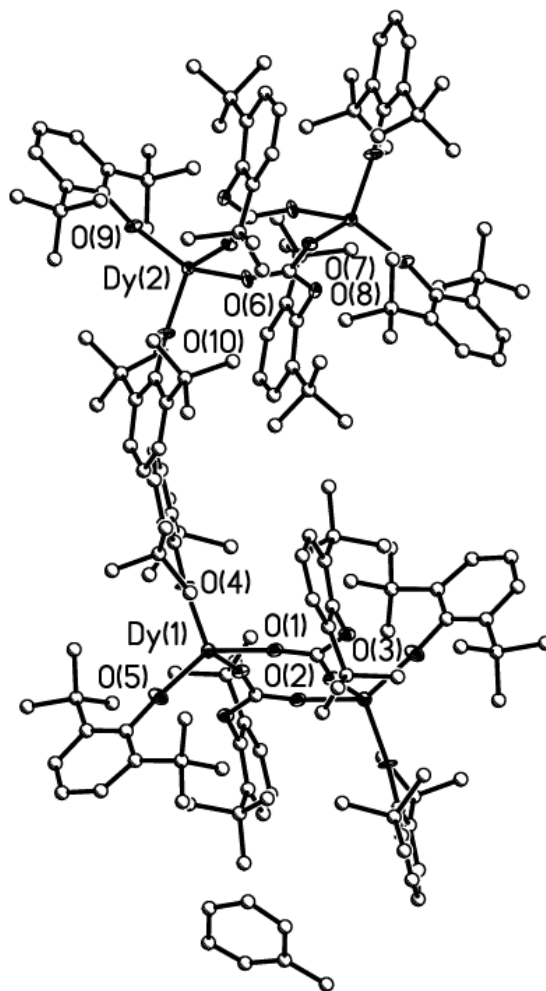
Figure 27. Structure plot of **14**. Thermal ellipsoids of heavy atoms are drawn at the 30% level and carbon atoms are shown as balls and sticks for clarity.
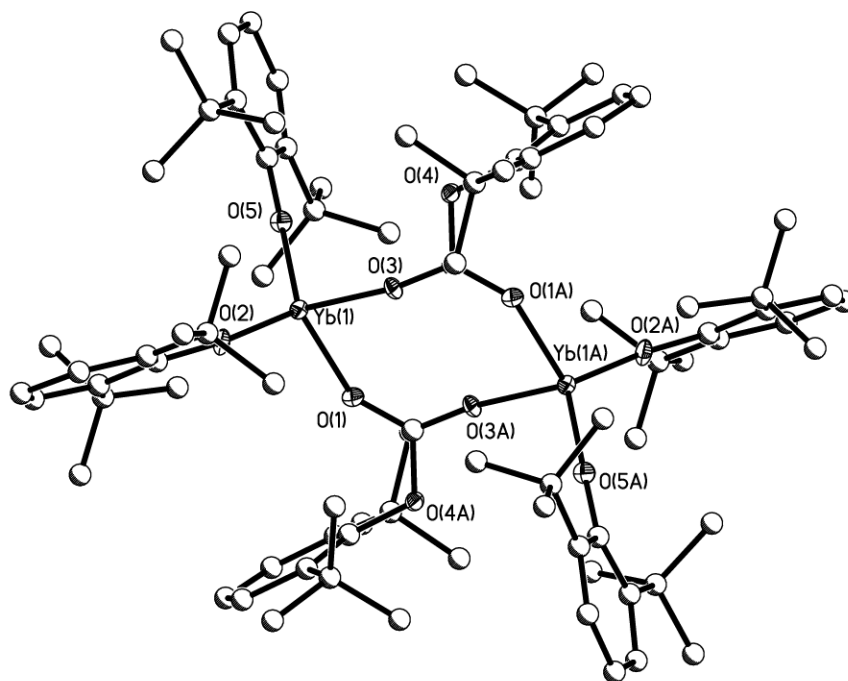
Figure 28. Structure plot of **15**. Thermal ellipsoids of heavy atoms are drawn at the 30% level and carbon atoms are shown as balls and sticks for clarity.
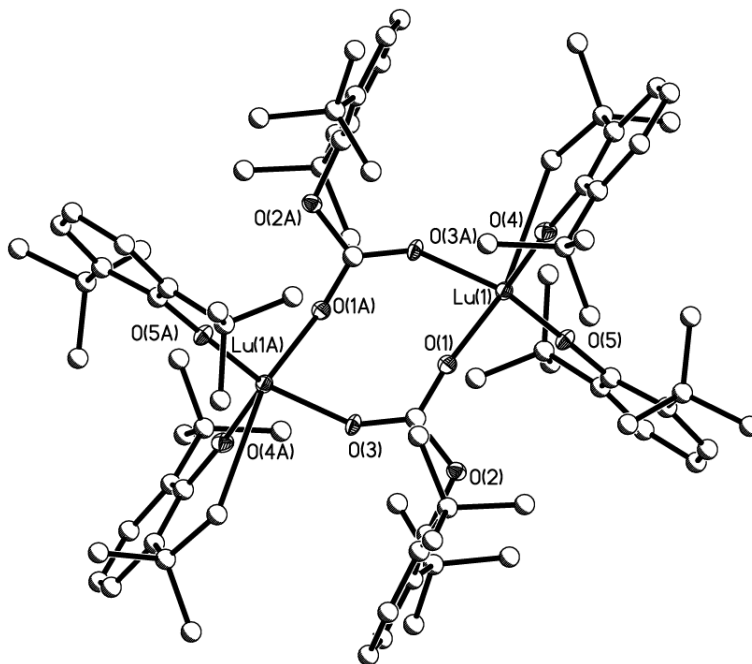
Compounds **12** and **13** contain two independent molecules in the unit cell in addition to one toluene molecule in the lattice while the others are solvent-free. Disorder in two of the *t*-butyl groups for **14** resulted in large thermal ellipsoids, which made locating the hydrogen atoms on two of the methyl groups difficult. Due to the disorder around the metal atom, the Yb atom was in close proximity with two methyl groups, allowing an Yb-C interaction in the model. Compound **15** has the same disorder in two *t*-butyl groups and results in difficulty in locating hydrogen atoms on the disordered methyl groups. Therefore, an interaction between the Lu and methyl carbon seem to be present. However, no agostic interactions are present in the FT-IR spectra for **14** or **15** and so the

Ln-C interaction can be attributed to the disorder in the structure model. For direct comparisons of the novel compounds **11 - 15,** average bond distances and angles of interest are tabulated in **Table 5**.

4.4.3.3 Solution Behavior of [Ln(μ-O$_2$C-DBP)(DBP)$_2$]$_2$ Species

The CO_2 insertion products (**11 - 15**) suffered from limited solubility, and coupled with the expected slow relaxation times of Ln species made obtaining useful NMR spectra difficult. The ^{13}C NMR resonance assigned to carbonate ligands are reported to be near δ 190.0 ppm.[107] Extended data collection attempts did not improve the signal to noise ratio and no measureable signals could be observed. Solid state NMR spectroscopy was not done for any of the compounds because the packing disorders that alkoxides can exhibit based on restricted rotation that yields erroneous peaks and no useful information for the compounds.[81]

4.4.4 High Pressure Reactions of CO$_2$ into Ln(OR)$_3$ Species

For low pressures of CO_2, insertion occurred into only one Ln-O bond of Ln(OR)$_3$, forming an alkoxycarbonate complex. To explore whether the compound could incorporate more CO_2into the other Ln-O bonds, elevated pressures were used for attempted insertion into **8**. This compound was chosen for the study because of its availability in large quantities. For the increase the CO_2 pressure reactions a 53 mM solution of **8** in toluene was prepared and transferred to the glass reaction vessel equipped with a pop-top regular apparatus (**Figure 8**). The vessel was transferred from the glovebox to Schlenk line where the CO_2 was attached to the regulator. After evacuation of the lines, CO_2 regulated at approximately 90 psig was introduced to the stirring

solution for 1 hr. The colorless solution turned dark brown after 30 min. with no further color change noticed. Crystals were obtained upon slow evaporation of the solution and yielded an identical structure solution as **13**. Therefore elevated pressure of CO_2 did *not* favor additional CO_2 insertion into more Ln-O bonds. Further characterization of this product was not done since the crystal structure match that of the previous result.

4.4.5 CO$_2$ Insertion into Mixed Amide/Alkoxide

4.4.5.1 Synthesis

As previously stated the isolation of the mixed amide/alkoxide species yielded the full alkoxide or amide upon crystallization. Attempts to monitor the preference of CO_2 insertion into either an Ln-OR or Ln-NR bond in a compound that contains both groups was still of interest. Therefore, CO_2 insertion was done on the *in-situ* generated product. Following the procedure for CO_2 insertion at low pressures described above we obtained **16**. The compound formed in extremely low yield (a single crystal was isolated and X-ray diffraction data were collected) and rigorous attempts to reproduce this species proved to be difficult and were abandoned with no further results. FT-IR was also done on the compound but due to the low quantity further characterization could not be completed.

4.4.5.1.1 Analytical Evaluation

The low yield of compound **16** allowed for X-ray diffraction on a single crystal and FT-IR of the bulk material. In the FT-IR spectrum, a sharp peak at 1653 cm^{-1} was observed for O$_2$COR ligand (**Figure 29**). However, due to the complexity of the spectra, the CO peak that indicates bridging O$_2$COR ligand could not be identified. In addition, a broad OH stretch was observed at 3500 cm^{-1} that could be attributed to hydroxides in the

structure or the presence of free ligand (*H*-DBP) or water in the sample. Both examples are discussed further in the crystal structure analysis below.

Figure 29. FT-IR spectra plot of **16.**
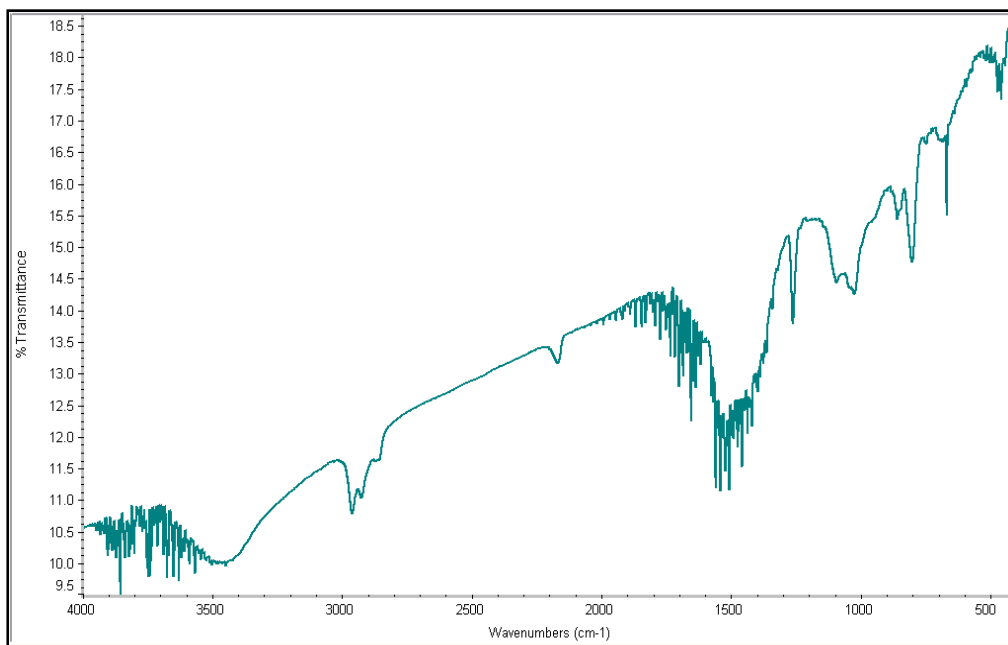
4.4.5.2   Crystal Structure and Metrical Data for CO_2 Insertion into Amide/alkoxide

Crystal structure parameters for the 'best-fit' structure of **16** are listed in **Table 4**. For the tetranuclear complex the coordination around the Sm atoms alternate between 6 and 7-coordinate. The ligands of the 7-coordinate Sm atoms are arranged in distorted pentagonal bipyramid geometry while the 6-coordinate Sm atoms have the ligands in a distorted octahedral arrangement. Each Sm has one terminal DBP ligand and the 7-

coordinate Sm has a THF solvent molecule bound. The Sm atoms are bridged in a μ_2 fashion by alternating O_2C-DBP or what appears to be a μ_2-oxo ligand. In addition two quadruply bridging CO_3^{-2} or NO_3^- moieties (could not confirm identification by crystallography) link the four Sm atoms (**Figure 30**).

Figure 30. Structure plot of **16**. Thermal ellipsoids of heavy atoms are drawn at the 30% level and carbon atoms are shown as balls and sticks for clarity.
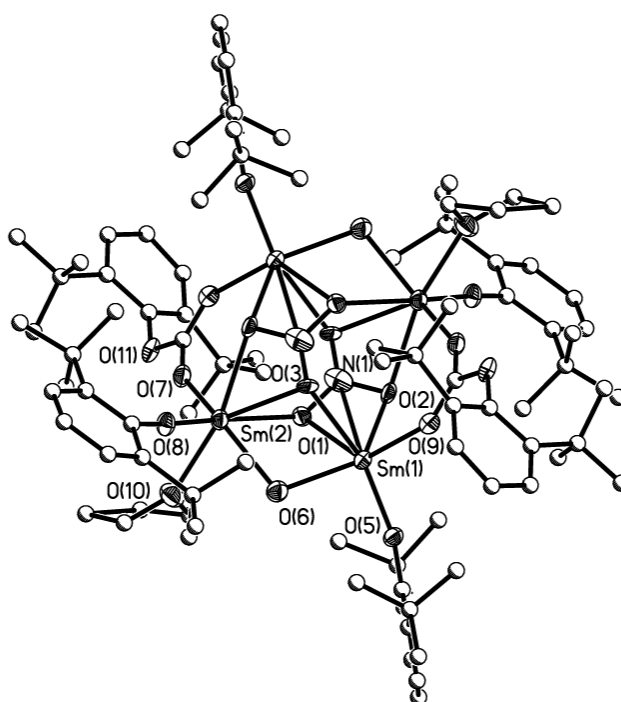
The identity of the two groups that link all four Sm atoms is ambiguous; however, there are three possibilities for this structure that make it chemically charge-balanced: 1) two μ_4-CO_3^{-2} ligands bridge together the four Sm^{+3} atoms, requiring the two lone bridging oxygen atoms to be hydroxides; 2) two μ_4-NO_3^- ligands bridge the four Sm^{+3} atoms, requiring the oxygen atoms to be oxo's, or 3) the compound is an equimixture of Sm^{+2}/Sm^{+3} metal centers, with bridging μ_4-CO_3^{-2} ligands that require the oxygens again

to be hydroxides to balance the charge. Location of possible hydrogen atoms on any

oxygen atoms could not be achieved in the crystal structure. In addition, changing from

CO_3^{-2} to NO_3^- during structure solutions did not change the refinement value, R1 =

6.96%. The unknown moiety is planar which is characteristic of CO_3^{-2}. For nitrates, the

lone pair of electrons on the nitrogen can force the geometry from trigonal planar to

pyramidal. However, since the group is multi-bridging the Sm atoms, a planar geometry

is observed and cannot be assigned to a NO_3^- or CO_3^{-2} without further analysis. A

comparison of bond distances and angles for each complex (NO_3^- or CO_3^{-2}) was tabulated

in **Table 3** resulting in insignificant differences.

Table 3. Metrical parameters for **16**.

Bond distances and angles (av.)	16 (NO_3^-)	Bond distances and angles (av.)	16 (CO_3^{-2})
Ln-OR	2.09	**Ln-OR**	2.08
Ln-O (for $\mu_2\eta^2$- O_2C-DBP)	2.34	**Ln-O** (for $\mu_2\eta^2$-CO_2DBP)	2.34
Ln- O_3N	2.50	**Ln- O_3C**	2.50
Ln-O (for oxo)	2.30	**Ln-O** (for oxo)	2.30
RO-Ln-O (for $\mu_2\eta^2$- O_2C-DBP)	106.85	**RO-Ln-O** (for $\mu_2\eta^2$- O_2C-DBP)	101.02
O-Ln-OR	96.90	**O-Ln-OR**	96.90
Sm-O-Sm	106.80	**Sm-O-Sm**	107.01
Sm-O_3N-Sm	92.85	**Sm-O_3C-Sm**	105.5

Chemically, arguments could be made for each structure option; therefore, further analysis by FT-IR analysis was done. The carbonate ligand stretch is present but CO_3^{-2} and the O_2C-DBP ligand will have similar IR stretches. In addition, the OH stretch observed could account for the two bridging hydroxides needed in the structure if the triply-bridging group is labeled a carbonate. However, if that group is assigned as a nitrate moiety, then no hydroxides are needed for charge balance. There was the possibility that free ligand (*H*-DBP) was present in the sample during data collection which would give an OH stretch. Therefore, the FT-IR data does not definitively confirm any of these structure types and due to the low yield and low reproducibility of this compound no definitive statements can be made at this time.

4.5 Conclusion

4.5.1 Discussion of CO_2 Insertion into Ln(OR)₃ Complexes

The compounds resulting from this research have proved to be very interesting. We have shown that at low pressures CO_2 selectively inserts into only some of the Ln-O bonds of Ln(OR)₃ to form [Ln(μ-O_2C-DBP)(DBP)₂]₂. This occurred independent of the atomic radii. Even at higher CO_2 pressures, insertion into more Ln-O bonds could not be achieved. The study of insertion into a mixed amide/alkoxide resulted in a unique complex with what appeared to be a triply bridging CO_3^{-2} ligand present. There are only two other similar crystallographically-characterized examples in the literature of complexes related to ours; however, neither of these were formed by CO_2 insertion into alkoxide bonds.[107, 108] The fact that CO_2 does not insert into all of the Ln-OR bonds is a promising feature. This suggests that insertion into these precursors might be preventable

if the correct ligand set is chosen. In addition, if a CO_2 resistant precursor could be achieved thermal processing into the desired ceramic metal oxides would proceed at much lower temperatures *via* bypassing carbonate formation. This would be very important for materials research because the cost of thermal budgets could be minimized. In addition, undesired fluoride-containing compounds that have the possibility to evolve $F_2(g)$ or HF can be avoided if thermal processing of alkoxides that do not evolved though a carbonate intermediate were achieved.

4.5.2 Implications of Future Research

Since an overall goal is to decrease undesired CO_2 insertions into metal alkoxides during processing into ceramic materials, finding precursors that at elevated temperatures and atmospheric conditions are even more resistant to insertion is of interest. To achieve this, there are several variables that can be manipulated in order to determine the proper precursors to allow this goal to be reached. A first step in future work would be to test other ligand sets under the same conditions that were used for this research to see if changing the electronics or sterics around the metal could affect CO_2 insertion. Results from using less bulky ligands such as $-N(SiMe_3)_2$ appear to give products that result from CO_2 inserting into all of the Ln-N bonds, eliminating various organic compounds, and then oligomerizing into multinuclear amorphous materials. Increasing the ligand bulk around the metal as shown in this research can increase the possibility to crystallize the metal-containing CO_2 insertion product by reducing the oligomerization process after CO_2 insertion occurs.

A ligand set that would be of interest to study CO_2 insertion reactions are sterically hindering substituted phenols. It was shown that the steric bulk of *H*-DBP was able to prevent CO_2 insertion into most Ln-O bonds, and so altering the steric bulk of the substituents around the phenol ring might eliminate insertion entirely. A first set of substitutions would be to replace the *t*-butyl groups with phenyl groups (**Figure 31a**). The phenyl groups would significantly increase the Tolman cone angle from ~110° (DBP) to ~150°. In addition, the phenyl substituents may be close enough for π-interactions with the metal center, decreasing the reactive sites available on the metal. Further substitutions on the rings by using methyl, *t*-butyl, or additional phenyl groups would increase the overall electron donation capability of the ligand to the metal center making it more difficult to activate the Ln-O bond by CO_2 insertion (**Figure 31b, c and d**).

Figure 31. Schematic representation of **a)** DPP: 2,6-diphenylphenol, **b)** 3,5-dimetylDPP: 2,6-diphenyl-3,5-dimethylphenol, and **c)** 3,5-diBu*t*DPP**:** 2,6-diBu*t*-3,5-dimethylphenol , **d)** 3,5-diphenylDPP: 2,3,5,6-tetraphenylphenol
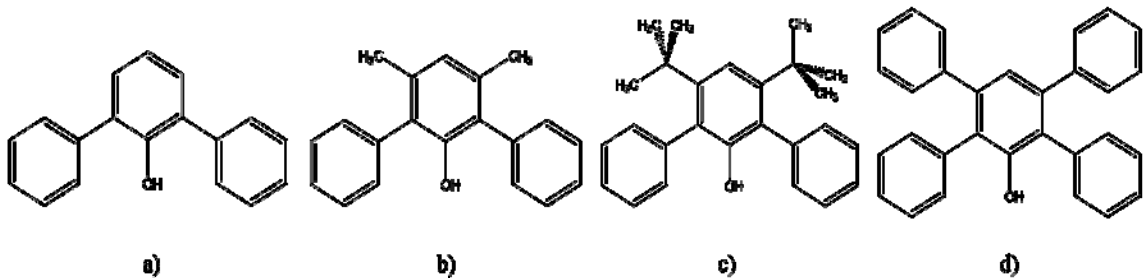
For some of the Ln^{+3} cations, structures that contain these ligands have been explored to yield fully-substituted monomeric species.[109-112] The compounds with ligand (**a**) all

posses metal-η-interactions with one or more phenyl ring substituents.[110-112] CO_2 insertion reactions with these Ln compounds could give further confirmation that changing the sterics of the ligand decreases the reactivity of insertion.

Another possible family of ligands that might be of interest for this study is the group of solvent-like, substituted methanol derivatives termed *H*-OR*, such as a) thiophene methanol (*H*-OTPM); b) tetrahydrofuran methanol (*H*-OTHF); or c) pyridine methanol (*H*-OPy) (**Figure 32**).[113]

Figure 32. Schematic representation of *H*-OR*
Ligands **a)** *H*-OTPM, **b)** *H*-OTHF, and **c)** *H*-OPy

a)　　　　　　　　　b)　　　　　　　　　c)
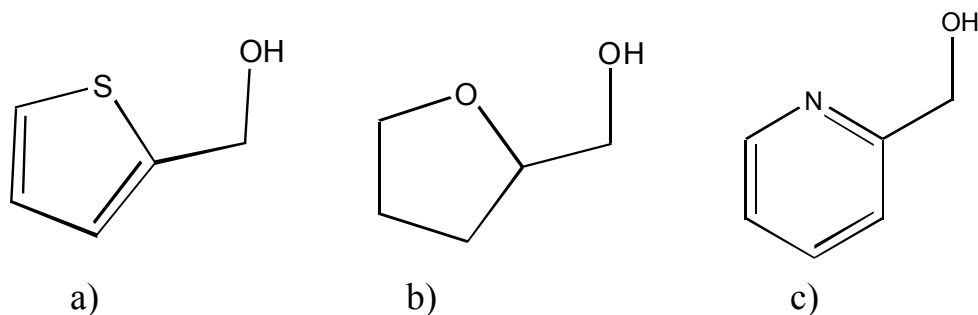
These ligands were termed OR* to differentiate them from typical monodentate alkoxides (OR). They are unique ligands because of their potential to bind to metals in a bidentate fashion, thus filling coordination sites around the metal and altering the electronics without significantly depleting the charge of the metal center. It has been shown in related chemistry that the OR* ligand can help prevent oligomerization of the final products as they can also shut down reactivity on parts of the metal center.[113] This concept is analogous to Cp ligands that have been used in organometallic chemistry for many years for this purpose. If fully-substituted Ln(OR*)$_3$ could perhaps be made that

could shut down all reactivity at the metal center, thus totally eliminating CO_2 insertion into Ln-O bonds. Examples of "CpLn" complexes with bidentate ligand, ε-caprolactamate, have been explored for CO_2 insertion as previously mentioned.[114] First, the dimeric precursor, $[(C_5H_4Me)_2Y(\mu\text{-}\varepsilon\text{-caprolactamate})]_2$, was reacted with CO_2 at ambient temperature for 24 hr but no reaction occurred.[114] However, when monomeric $(Cp^*)_2Y(\varepsilon\text{-caprolactamate})$ was left under CO_2 for 3 hr the product generated was insertion into the Y-N bond to yield $[(C_5Me_5)_2Y(\mu\text{-}O_2CNC_6H_{10}O)]_2$.[78] Since yttrium has no f-electrons the electronic properties can be drastically different than the other members of the Ln family. It would be of interest to synthesize the Ln analogues of Evans' compound for CO_2 insertion to determine if the reactivity is altered. The coordinated Cp groups also play an important role in the reactivity of these complexes due to their ability to shut down coordination sites on half the metal centers, ultimately preventing oligomerization of the products. However, it has been shown that CO_2 can insert into Ln-Cp bonds.[80] Therefore, developing compounds that mimic "CpLn(ε-caprolactamate)" may well be achieved with the OR* ligand. From this ligand set, designing precursors that are completely resistant for CO_2 insertion could be possible. Bulky, bidentate ligands that have the ability to bridge metal centers and form dinuclear complexes are the most promising precursors for elimination of CO_2 insertion.

After CO_2 insertion-resistant $Ln(OR)_3$ species are developed the next step is to increase the temperature at which CO_2 is inserted. This would be more comparable to actual processing temperatures and would give a better indication about the amount of CO_2 that can insert into Ln-O bonds. Characterizing this product my single crystal X-ray diffraction might not be possible since heating up $Ln(OR)_3$ could initiate ligand

decomposition not allowing for single crystal growth to be achieved. However, other analytical methods could be utilized to identify the product such as FT-IR, powder X-ray diffraction, EA to name a few.

Finally, once a Ln(OR)$_3$ precursor that is totally resistant to CO_2 insertion is prepared it could be examined by calcination under atmospheric conditions to test for carbonate formation throughout the process. Custom-designed precursors can make processing for materials applications more cost effective (process at lower temperature) and more efficient (fewer unwanted carbonate byproducts). Therefore, future studies to generate these types of precursors are of great interest.

5. APPENDICES

5.1 *Appendix A: TABLES*

Table 4. Crystallography data collection parameters for **7**, **9 - 16**. note: crystallography data for **1 - 6**, **8** are reported in the literature.[4-8, 65, 67]

Compound	7	9	10	11	12•tol
Chem. Form.	$C_{42}H_{63}O_3Sm$	$C_{42}H_{63}O_3Yb$	$C_{42}H_{63}Lu\ O_3$	$C_{86}Ce_2H_{126}O_{10}$	$C_{86}H_{126}O_{10}Sm_2•$ C_7H_8
Form. weight	766.36	789.00	790.93	1600.18	1712.70
temp (K)	173(2)	173(2)	173(2)	173(2)	173(2)
space group	Monoclinic, P2(1)	Monoclinic, P2(1)/c	Monoclinic, P2(1)/c	Triclinic, P1	Monoclinic, P2(1)/c
a (Å)	11.2751(16)	11.1188(12)	11.1133(14)	12.446(3)	25.770(4)
b (Å)	31.759(5)	31.937(3)	31.971(4)	13.141(4)	17.637(3)
c (Å)	11.6134(16)	11.6383(12)	11.5971(14)	13.630(4)	21.183(3)
α (deg)				69.904(7)	
β (deg)	105.031(2)	104.345(2)	104.368(2)	75.744(6)	95.986(3)
γ (deg)				76.311(6)	
V ($Å^3$)	4016.3(10)	4004.0(7)	3991.6(8)	2000.4(9)	9576(3)
Z	2	4	4	1	4
$D_{calc'd}(Mg/m^3)$	1.267	1.322	1.316	1.321	1.188
μ,(Mo, Kα)(mm^{-1})	1.496	2.370	2.507	1.179	1.265
R1[a](%)(all data)	3.72(3.85)	5.56(8.04)	4.18(4.72)	9.33 (15.16)	5.12(6.56)
wR2[b](%)(all data)	9.39(9.66)	13.94(15.67)	11.51(12.04)	17.19 (18.33)	11.54(12.1)

Table 4 (Continued)

Compound	13•tol	14	15	16
Chem. Form.	$C_{86}H_{126}Dy_2O_{10}$ • C_7H_8	$C_{86}H_{126}O_{10}Yb_2$	$C_{86}H_{126}Lu_2O_{10}$	$C_{94}H_{142}N_2O_{20}Sm_4$
Form. weight	1737.00	1666.02	1669.88	2221.50
temp (K)	173(2)	173(2)	173(2)	173(2)
space group	Monoclinic, P2(1)/c	Monoclinic, P2(1)/n	Monoclinic, P2(1)/n	Monoclinic, P2(1)/n
a (Å)	25.59(6)	14.5845(18)	14.6047(16	14.314(3)
b (Å)	17.74(4)	14.8159(19)	14.8216(16)	22.781(4)
c (Å)	21.05(5)	20.038(3)	20.017(2)	16.321(3)
α(deg)				
β (deg)	95.59(4)	108.233(2)	108.078(2)	112.132(4)
γ (deg)				
V (Å^3)	9509(41)	4112.5(9)	4119.0(8)	4929.8(15)
Z	4	2	2	2
$D_{calc'd}$(Mg/m^3)	1.213	1.340	1.345	1.497
μ,(Mo, Kα)(mm^{-1})	1.610	2.314	2.437	2.412
R1[a] (%) (all data)	10.32 (11.32)	6.64(10.52)	4.67(7.71)	6.95(14.02)
wR2[b](%) (all data)	23.52(23.89)	13.89(15.38)	7.93(8.74)	12.86(15.38)

[a]R1 $= \Sigma \mid \mid F_o \mid - \mid F_c \mid \mid / \Sigma \mid F_o \mid$ x 100   [b]wR2 $= [\Sigma$ w $(F_o^2 - F_c^2)^2 / \Sigma (w \mid F_o \mid^2)^2]^{1/2}$ x 100.

Table 5. Metrical parameters for **7**, **9- 15**.

Bond distances and angles (av.)	7	9	10	11
Ln-OR	2.11	2.02	2.07	2.13
RO-Ln-OR	110.37	113.81	112.30	233.2
Ln-O (for chelate $\mu_2\eta^3$- O_2C-DBP)	----------	----------	----------	2.45
Ln-O (for bridge $\mu_2\eta^3$- O_2C-DBP)	----------	----------	----------	2.59
O-Ln-O (for chelate $\mu_2\eta^3$-O)	----------	----------	----------	51.55
O-Ln- O (for bridge $\mu_2\eta^3$-O)	----------	----------	----------	67.9
Ln-O-Ln (for $\mu_2\eta^3$-O)	----------	----------	----------	112.05
	12	**13**	**14**	**15**
Ln-OR	2.10	2.05	2.02	2.01
Ln-O (for $\mu_2\eta^2$- O_2C-DBP)	2.30	2.26	2.16	2.15
RO-Ln-OR	108.09	113.10	119.10	118.33
RO-Ln-$\mu_2\eta^2$-O	113.17	112.00	110.43	110.48
O-Ln-O (for $\mu_2\eta^2$-O)	96.14	92.98	91.80	92.63

---- bond distance or angle is not present in structure

6. REFERENCES

1.   Behr, A., *Angewandte Chemie International Edition* **1988,** *27*, 661.

2.   Palmer, D. A.; Van Eldik, R., *Chemical Reviews* **1983,** *83*, 651.

3.   Yin, X.; Moss, J. R., *Coordination Chemistry Reviews* **1999,** *181*, 27.

4.   Niemeyer, M., *Zeitschrift für Anorganische und Allgemeine Chemie* **2002,** *628*, 647.

5.   Rees Junior, W. S.; Just, O.; Van Derveer, D. S., *Journal of Materials Chemistry* **1999,** *9*, 249.

6.   Secarel, G.; Wiemer, C.; Fanciulli, M.; Fedushkin, I. L.; Fukin, G. K.; Domrachev, G. A.; Lebedinskii, Y.; Zenkevich, A.; Pavia, G., *Zeitschrift für Anorganische und Allgemeine Chemie* **2007,** *633*, 2097.

7.   Boyle, T. J.; Bunge, S. D.; Clem, P. G.; Richardson, J.; Dawley, J. T.; Ottley, L. A. M.; Rodriguez, M. A.; Tuttle, B. A.; Avilucea, G. R.; Tissot, R. G., *Inorganic Chemistry* **2005,** *44*, 1588.

8.   Stecher, H. A.; Sen, A.; Rheingold, A. L., *Inorganic Chemistry* **1988,** *27*, 1130.

9.   Universal Industrial Gases http://www.uigi.com/carbondioxide.html   Carbon Dioxide Properties, Uses, Applications. (accessed October 12, 2009).

10.   McIntyre, P. C.; Cima, M. J.; Ng, M. F., *Journal of Applied Physics* **1990,** *68*, 4183.

11.   Schwartz, R. W., *Chemistry Materials* **1997,** *9*, 2325.

12.   Cima, M. J.; Schneider, J. S.; Peterson, S. C., *Applied Physical Letters* **1968,** *53*, 710.

13.   Ito, T.; Kato, M., *Inorganic Chemistry* **1985,** *24*, 509.

14.   Kemp, R. A.; Tang, Y.; Kassel, W. S.; Zakharov, L. N.; Rheingold, A. L., *Inorganic Chemistry* **2005,** *44*, 359.

15.   Kemp, R. A.; Tang, Y.; Zakharov, L. N.; Rheingold, A. L., *Organometallics* **2004,** *23*, 4788.

16.   Cotton, F. A.; Wilkinson, G., *Advanced Inorganic Chemistry*. 5 ed.; Wiley: New York, 1988.

17.   Seitz, M.; G., O. A.; Raymond, K. N., *Journal of American Chemical Society* **2007,** *129*, 11153.

18. Mioduski, T., *Journal of Radioanalytical and Nuclear Chemistry*. Akadémiai Kiadó, co-published with Springer Science+Business Media B.V., Formerly Kluwer Academic Publishers B.V.: 1993; Vol. 179, p 371.

19. Boyle, T. J.; Hernandez-Sanchez, B. A.; Lambert, T. N.; Daniel, S. D.; Oliver, J. M.; Wilson, B. S.; Lidke, D. S.; Andrews, N. A., *IEEE Transactions of Nanobioscience* **2006,** *5*, 222.

20. Boyle, T. J.; Pratt, H. D.; Hernandez-Sanchez, B. A.; Lambert, T. N.; Headley, T. J., *Journal Of Material Science* **2007,** *42*, 2792.

21. Bochkarev, M. N.; Fedorova, E. A.; Rad'kov, Y. F.; Kalinina, G. S.; Khorshev, S. Y.; Razuvaev, G. A., *Doklady Akademii Nauk SSSR* **1984,** *279*, 1386.

22. Costes, J. P.; Dahan, F.; Dupuis, A.; Laurent, J. P., *New Journal of Chemistry* **1998,** *200*, 1525.

23. Costes, J. P.; Dahan, F.; Wernsdorfer, W., *Inorganic Chemistry* **2006,** *45*, 5.

24. Rad'kov, Y. F.; Fedorova, E. A.; Khorshev, S. Y.; Kalinina, G. S.; Bochkarev, M. N.; Razuvaev, G. A., *Journal of General Chemistry of the USSR* **1986**, 336.

25. Baisch, U.; Pagano, S.; Zeuner, M.; W., S., *European Journal of Inorganic Chemistry* **2006**, 3517.

26. Carey, F. A.; Sundberg, R. J., *Advanced Organic Chemistry*. Fourth ed.; Kluwer Academic/Plenum New York, **2000**.

27. McMurry, J., *Organic Chemistry*. 6th ed.; Brooks/Cole-Thomson Learning: Belmont, **2004**.

28. Lackner, K. S.; Park, A. H.; Fan, L. S., *Carbon Dioxide Capture and Disposal: Carbon Sequestration* **2005**.

29. Dikie, D.; Parks, M. V.; Kemp, R. A., *Angewandte Chemie International Edition* **2008,** *47*, 9955.

30. Belforte, A.; Dell' Amico, D. B.; Calderazzo, F.; Devillers, M.; Englert, U., *Inorganic Chemistry* **1993,** *32*, 2282.

31. Caudle, M. T.; Nieman, R. A.; Young, V. G., *Inorganic Chemistry* **2001,** *40*, 1571.

32. Cotton, F. A.; Chisholm, M. H.; Extine, M. W.; Rideout, D. C., *Inorganic Chemistry* **1978,** *17*, 3536.

33. Cummins, C. C.; Cotton, F. A.; Murillo, C. A.; Mendiratta, A.; Ibragimov, S. A., *Inorganic Chemistry* **2006,** *45*, 4328.

34.   Horley, G. A.; Mahon, M. F.; Molloy, K. C., *Inorganic Chemistry* **2002,** *41*, 5052.

35.   Snaith, R.; Davies, R. P.; Raithby, P. R., *Organometallics* **1996,** *15*, 4355.

36.   Srivastava, R. S.; Singh, G.; Nakano, M.; Osakada, K.; Ozawa, F.; Yamamoto, A., *Journal of Organometallic Chemistry* **1993,** *451*, 221.

37.   Yang, K. C.; Chang, C. C.; Yeh, C. S.; Lee, G. H.; Peng, S. M., *Organometallics* **2001,** *20*, 126.

38.   Calderazzo, F.; Abis, L.; Dell' Amico, D. B.; Caminiti, R.; Garbassi, F.; Ianelli, S.; Pelizzi, G.; Robino, P.; Tomei, A., *Journal of Molecular Catalysis A: Chemical* **1996,** *108*, L113.

39.   Calderazzo, F.; Ianelli, S.; Pampaloni, G.; Pelizzi, G.; Sperrle, M., *Journal of the Chemical Society Dalton Transactions* **1991**, 693.

40.   Arimondo, P. B.; Calderazzo, F.; Englert, U.; Maichle-Mossmer, C.; Pampaloni, G.; Strahle, G., *Journal of the Chemical Society Dalton Transactions* **1996**, 311.

41.   Dell' Amico, D. B.; Calderazzo, F.; Dell'Innocenti, M.; Guldenpfennig, B.; Ianelli, S.; Pelizzi, G.; Robino, P., *Gazzetta Chimica Italiana* **1993,** *123*, 283.

42.   Immirzi, A.; Musco, A., *Inorganica Chimica Acta* **1977,** *22*, L35.

43.   Ashworth, T. V.; Singleton, E., *Journal of the Chemical Society, Chemical Communications* **1976**, 204.

44.   Inoue, S.; Nukui, M.; Kojima, F., *Chemical Letters* **1984**, 619.

45.   Puddephatt, R. J.; Aye, K. T.; Ferguson, G.; Lough, A. J., *Angewandte Chemie International Edition* **1989,** *28*, 767.

46.   Dussart, Y.; Harding, C.; Dalgaard, P.; McKenzie, C.; Kadirvelraj, R.; McKee, V.; Nelson, J., *Journal Chemical Society, Dalton Transition* **2002**, 1704.

47.   Kitajima, N.; Hikichi, S.; Tanaka, M.; Moro-oka, Y., *Journal of American Chemical Society* **1993,** *115*, 5496.

48.   Funaioli, T.; Biagini, P.; Zanazzi, P. F.; Fachinetti, G., *Gazzetta Chimica Italiana* **1991,** *121*, 321.

49.   Lu, T.-B.; Chen, J.-M.; Wei, W.; Feng, X.-L., *Chemistry- an Asian Journal* **2007,** *2*, 710.

50.   Hidai, M.; Hikita, T.; Uchida, Y., *Chemical Letters* **1972**, 521.

51.   Razuvaev, G. A.; Vyshinskaya, L. I.; Drobotenko, V. V.; Malkova, G. Y.; Vyshinskii, N. N., *Journal of Organometallic Chemistry* **1982,** *239*, 335.

52. Ovchinnikova, N. A.; Glushkova, M. A.; Buslaev, Y. A., *Corrdination Chemistry* **1979,** *5*, 385.

53. Fachinetti, G.; Floriani, C.; Chiesi-Villa, A.; Guastini, C., *Journal of American Chemical Society* **1979,** *101*, 1767.

54. Chisholm, M. H.; Cotton, F. A.; Extine, M. W.; Reichert, W. W., *Journal of American Chemical Society* **1978,** *100*, 1727.

55. Ito, H.; Ito, T., *Acta Crystallography, Section C: Crystal Structure Communication* **1985,** *41*, 1598.

56. Buffin, B. P.; Arif, A. M.; Richmond, T. G., *Journal of the Chemical Society, Chemical Communications* **1993**, 1432.

57. Darensbourg, D. J.; Sanchez, K. M.; Reibensoies, J. H.; Rheingold, A. L., *Journal of the American Chemical Society* **1989,** *111*, 7049.

58. Darensbourg, D. J.; Mueller, B. L.; Bischoff, C. J.; Chojnacki, S. S.; Reibenspies, J. H., *Inorganic Chemistry* **1991,** *30*, 2418.

59. Chisholm, M. H.; Extine, M. W., *Journal of American Chemical Society* **1975,** *97*, 5625.

60. Mandal, S. K.; Ho, D. M.; Orchin, M., *Organometallics* **1993,** *12*, 1714.

61. Chisholm, M. H.; Cotton, F. A.; Extine, M. W.; Rideout, D. C., *Inorganic Chemistry* **1979,** *18*, 120.

62. Hursthouse, M. B.; Arunasalam, V. C.; Baxter, I.; Darr, J. A.; Drake, S. R.; Malik, A.; Mingos, M. P., *Polyhedron* **1998,** *17*, 641.

63. Dell'Amico, D. B.; Calderazzo, F.; Gingl, F.; Labella, L.; Strahle, J., *Gazzetta Chimica Italiana* **1994,** *124*, 375.

64. Andersen, R. A.; Templeton, D. H.; Zalkin, A., *Inorganic Chemistry* **1978,** *17*, 2317.

65. Bradley, E. D.; Clark, D. L.; Gordon, J. C.; Hay, P. J.; Keogh, W.; Poli, R.; Scott, B. L.; G., W. J., *Inorganic Chemistry* **2003,** *42*, 6682.

66. Ghotra, J. S.; Hursthouse, M. B.; welch, A. L., *Chemical Communications* **1973**, 669.

67. Herrmann, W. A.; Andwander, R.; Munck, F. C.; Scherer, W.; V., D.; Huber, N. W.; Artus, G. R., *Zeitschrift für Naturforschung B. A Journal of Chemical Sciences* **1994,** *49*, 1789.

68.   Hitchcock, P. B.; Hulkes , A. G.; lappert, M. F.; Li, Z., *Dalton Transition* **2004**, 129.

69.   Sheng, E.-H.; Yang, G.-S.; Dong, B.-P., *Natural Science* **2002,** *25*, 254.

70.   Sundermeyer, J.; Khvorost, A.; Harms, K., *Acta Crystallography., Section. E: Structure Report Online* **2004,** *60*, m1117.

71.   Abram, U.; Dell'Amico, D. B.; Calderazzo, F.; Della Porta, C.; Englert, U.; Marchetti, F.; Merigo, A., *Chemical Communications* **1999**, 2053.

72.   Baisch, U.; Dell'Amico, D. B.; Calderazzo, F.; Labella, L.; Marchetti, F.; Merigo, A., *European Journal of Inorganic Chemistry* **2004**, 1219.

73.   Baisch, U.; Dell'Amico, D. B.; Calderazzo, F.; Labella, L.; Marchetti, F.; Vitali, D., *Journal of Molecular Catalysis A: Chemical* **2003,** *204*, 259.

74.   Baisch, U.; Schnick, W., *Zeitschrift für Anorganische und Allgemeine Chemie* **2003,** *629*, 2073.

75.   Dell'Amico, D. B.; Calderazzo, F.; Marchetti, F.; Perego, G., *Chemical Communications* **1979**, 1103.

76.   Dell'Amico, D. B.; Calderazzo, F.; Marchetti, F.; Perego, G., *Journal of the Chemical Society Dalton Transactions* **1983**, 483.

77.   Schumann, H.; Meese-Martscheffel, J. A.; Dietrich, A.; Gorlitz, F. H., *Journal of Organometallic Chemistry* **1992,** *430*, 299.

78.   Evans, W. J.; Fujimoto, C. H.; Ziller, J. W., *Organometallics* **2001,** *20*, 4529.

79.   Evans, W. J.; Seilbel, C. A.; Ziller, J. W., *Inorganic Chemistry* **1998,** *37*, 770.

80.   Evans, W. J.; Seilbel, C. A.; Ziller, J. W.; Doedens, F. H., *Organometallics* **1998,** *17*, 2103.

81.   Boyle, T. J.; Tribby, L. J.; Bunge, S. D., *European Journal of Inorganic Chemistry* **2006**, 4553.

82.   Bradley, D. C.; Chudzynska, H.; Hursthouse, M. B.; Motevalli, M., *Polyhedron* **1991,** *10*, 1049.

83.   Daniele, S.; Hubert-Pfalzgraf, L. G.; Hitchcock, P. B.; Lappert, M. F., *Inorganic Chemistry Communication* **2000,** *3*, 218.

84.   Gromada, J.; Mortreux, A.; Chenal, T.; Ziller, J. W.; Leising, F.; Carpentier, J. F., *European Journal of Inorganic Chemistry* **2002,** *8*, 3773.

85.   Boyle, T. J.; Ottley, L. A. M., *Chemical Reviews* **2008,** *108*, 1896.

86.   Bradley, D. C.; Ghotra, J. S.; Hart, F. A., *Journal of American Chemical Society, Dalton Transactions* **1973**, 1021.

87.   Eller, P. G.; Bradley, D. C.; Hursthouse, M. B.; Meek, D. W., *Corrdination Chemical Reviews* **1977,** *24*, 1.

88.   Chambers, J. L.; Smith, K. L.; Pressprich, M. R.; Jin, Z., *Bruker Advanced X-ray Solutions SMART for WNT/2000*. Version 5.625 ed.; Bruker Analytical X-ray Systems, Inc., Madision, WI, 2001.

89.   Sheldrick, G. M., *SHELXTL*. Version 6.1 ed.; Bruker Analytical X-ray Systems, Inc., Madison, WI, 2001.

90.   Sheldrick, G. M., *SAINTPLUS*. Volume 5.0 ed.; Bruker Analytical X-Ray Systems, Inc., Madison, WI, 2001.

91.   Amberger, H.; Reddmann, H.; Guttenberger, C.; Unrecht, B.; Zhang, L.; Apostolidis, C.; Walter, O.; Kanellakopulos, B., *Zeitschrift für Anorganische und Allgemeine Chemie* **2003,** *629*, 1522.

92.   Socrates, G., *Infrared and Raman Characteristic Group Frequencies: Tables and Charts*. third ed.; Wiley: West Sussex, 2001.

93.   Bradley, D. C.; Gitlitz, M. H., *Nature* **1968,** *218*, 353.

94.   Boyle, T. J.; Ottley, L. A. M.; Daniel, S. D.; Tribby, L. J.; Bunge, S. D., *Inorganic Chemistry* **2007,** *46*, 3705.

95.   Muller, T. E.; Mingos, M. P., *Transition Metal Chemistry* **1995,** *20*, 533.

96.   Bradley, D. C., *Chemical Reviews* **1989,** *89*, 1317.

97.   Caulton, K. G.; Hubert-Pfalzgraf, L. G., *Chemical Reviews* **1990,** *90*, 969.

98.   Chandler, C. D.; Roger, C.; Hampden-Smith, M. J., *Chemical Reviews* **1993,** *93*, 1205.

99.   Hubert-Pfalzgraf, L. G., *New Journal of Chemistry* **1987,** *11*, 663.

100.   Hou, Z.; Fujita, A.; Zhang, Y.; Miyano, T.; Yamazaki, H.; Wakatuski, Y., *Journal of American Chemical Society* **1998,** *120*, 757.

101.   Van Den Hende, J. R.; Hichcock, P. B.; Lappert, M. F., *Chemical Communications* **1994**, 1413.

102.   Xu, Z.; Zhang, Z.; Yao, Y.; Zhang, Y.; Shen, Q., *Inorganic Chemistry* **2007,** *46*, 9379.

103. Chaudhuri, P.; Pavlishchuk, V.; Birkelbach, F.; Weyhermuller, T.; Wieghardt, K., *Inorganic Chemistry* **2002,** *41*, 4405.

104. Samuelson, A. G.; Ghosh, R.; Nethaji, M., *Chemical Communications* **2003**, 2556.

105. Bradley, D. C.; Mehrotra, R. C.; Gaur, D. P., *Metal Alkoxides*. Academic Press: New York, 1978.

106. Turova, N. Y.; Turevskaya, E. P.; Kessler, V. G.; Yanovskaya, M. I., *The Chemistry of Metal Alkoxides*. Kluwer Academic Publishers: Boston, 2002.

107. Gardiner, M. G.; Davies, N. W.; Frey, A. S. P.; Wang, J., *Chemical Communications* **2006**, 4853.

108. Bombieri, G.; Benetollo, F.; Polo, A.; Fonda, K. K.; Vallarino, L. M., *Polyhedron* **1991,** *10*, 1385.

109. Deacon, G. B.; Fanwick, P. E.; Gitlits, A.; Rothwell, I. P.; Skelton, B. W.; White, A. H., *European Journal of Inorganic Chemistry* **2001**, 1505.

110. Deacon, G. B.; Nickel, S.; MacKinnon, P.; Tiekink, E. R. T., *Australian Journal of Chemistry* **1990,** *43*, 1245.

111. Deacon, G. B.; Tiecheng, F.; Forsyth, C. M.; Gitlits, A.; Hockless, D. C.; Shen, Q.; Skelton, B. W.; White, A. H., *Journal of the Chemical Society Dalton Transactions* **2000**, 961.

112. Deacon, G. B.; Tiecheng, F.; Skelton, B. W.; White, A. H., *Australian Journal of Chemistry* **1995,** *48*, 741.

113. Boyle, T. J.; Sewell, R. M.; Ottley, L. A. M.; Pratt, H. D.; Quintana, C. J.; Bunge, S. D., *Inorganic Chemistry* **2007,** *46*, 1825.

114. Shen, Q.; Wang, Y.; Mu, L.; Zhang, Y.; Sun, J., *Journal of Organometallic Chemistry* **2001,** *626*, 176.